Journal Name

Theoretical Characterization of the Surface Composition of Ruthenium Nanoparticles in Equilibrium with Syngas[†]

Lucy Cusinato,[a] Luis M. Martínez-Prieto,[a] Bruno Chaudret,[a] Iker del Rosal[a] and Romuald Poteau[*a]

A deeper understanding of the relation between experimental reaction conditions and the surface composition of nanoparticles is crucial in order to elucidate mechanisms involved in nanocatalysis. In the framework of the Fischer-Tropsch synthesis, a resolution of this complex puzzle requires a detailed understanding of the interaction of CO and H with the surface of the catalyst. In this context, the single- and co-adsorption of CO and H to the surface of a 1 nm ruthenium nanoparticle has been investigated with density functional theory. Using several indexes (d-band center, crystal overlap Hamilton population, density of states), a systematic analysis of the bond properties and of the electronic states has also been done, in order to bring an understanding of structure/property relationships at the nanoscale. The H:CO surface composition of this ruthenium nanoparticle exposed to syngas has been evaluated according to a thermodynamic model fed with DFT energies. Such ab initio thermodynamic calculations give access to the optimal H:CO coverage values under a wide range of experimental conditions, through the construction of free energy phase diagrams. Surprisingly, under the Fischer-Tropsch synthesis experimental conditions, and in agreement with new experiments, only CO species are adsorbed at the surface of the nanoparticle. These findings shed a new light on the possible reaction pathways underlying the Fischer-Tropsch synthesis, and specifically the initiation of the reaction. It is finally shown that the joint knowledge of the surface composition and of energy descriptors can help to identify possible reaction intermediates.

1 Introduction

Fischer-Tropsch synthesis (FTS) is a catalytic process that converts a mixture of carbon monoxide and dihydrogen in the gas phase into mainly linear hydrocarbons and water (eq. 1). It is known for around ninety years now[1] and it is still of high interest because of its ability to produce fuels with lower environmental impact, but higher financial costs, than regular production pathways.[2,3]

$$(2n+1)H_2 + nCO \longrightarrow C_nH_{2n+2} + nH_2O \qquad (1)$$
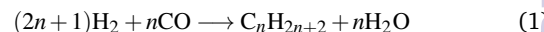
The FTS is assumed to proceed via three main processes: (i) the initiation step which corresponds to the coordination of CO and H_2 and the formation of the chain starter; (ii) the propagation step which involves different hydrogenation reactions as well as carbon-carbon coupling reactions leading to the growth of the hydrocarbon chain; (iii) the termination step corresponding to the desorption of the hydrocarbons and water.[2] Each step has its importance in the resulting products and several ways to achieve high selectivity towards long chain hydrocarbons have been studied both theoretically and experimentally.[4–7] The first step of the reaction is still debated as different mechanisms are usually proposed for the CO dissociation: the "carbide mecha-

[a] Université de Toulouse; INSA, UPS, CNRS; LPCNO (IRSAMC), 135 avenue de Rangueil, F-31077 Toulouse, France. Fax: 0033 56155 9697; Tel: 0033 56155 9664; E-mail: romuald.poteau@univ-tlse3.fr

nism" in which the adsorbed CO directly dissociates into C and O at the catalyst surface and are subsequently hydrogenated to CH_2 and H_2O, [1,8–15] or the H-assisted mechanism [13–19], such as the CO insertion mechanism proposed by Pichler and Schulz [20] as well as by Henrici-Olivé and Olivé [21] or the enol mechanism proposed by Storch *et al.*, [22] in which an H atom binds to the CO before the C – O activation leading to the formation of different intermediates like COH or HCO helping the CO dissociation.

Among the catalysts used, ruthenium surfaces have been widely studied, both theoretically and experimentally, regarding CO adsorption and dissociation [23,24] as well as H_2 adsorption [25,26] and H_2/CO co-adsorption. [27] Surfaces have been studied both for their own heterogeneous catalytic activities but also as models for nanoparticle with large facets, with or without special sites like step sites. Such sites have been evidenced as being of importance in the catalytic process, as their effect on the adsorption energies and dissociation barriers allows to facilitate reactions. [28] In the particular case of the Fischer-Tropsch synthesis, theoretical and experimental studies have evidenced the role of steps. Regarding the initiation step, the DFT computed energy barrier for CO dissociation drops from 54.3 kcal.mol^{-1} to 21.3 kcal.mol^{-1} when the dissociation occurs at a step site. [29] The blocking of the steps by carbon atoms resulting from the CO dissociation poisons the surface and prevent further CO dissociation under ultra high vacuum conditions, whereas step blocking no longer dominates CO dissociation at high CO pressure. [30]

Nanoparticles (NPs) have a periodicity much reduced compared to flat or stepped surfaces. Since they possess more surface irregularities and defective sites (Figure S1), they are good candidates as catalysts. In fact ruthenium nanoparticles (RuNPs) ranging from 1.3 nm to 2.9 nm have been experimentally studied as FTS catalysts in gaseous phase, showing the importance of the catalyst size and of the stabilizing ligands towards FTS activity. [31] Same conclusions were drawn for larger (4-23 nm) RuNPs. [32] Other RuNPs (1.2 nm to 5.2 nm) have been studied for FTS in aqueous phases demonstrating high selectivity towards oxygenated species on dense RuNP surfaces. [4] In the case of ultra small (∼1 nm) to small (≲3 nm) NPs, the edge/surface atoms or apex/surface atoms ratios are large. The "nanoparticle as an assembly of surfaces" model becomes less relevant, and very large metal clusters should rather be investigated.

The purpose of the study we propose here is to theoretically investigate the adsorption of H_2 or CO at the surface of ruthenium nanoparticles for several coverage values, as well as the H/CO co-adsorption, in order to give an insight into the optimal surface composition. We have considered a RuNP core with a diameter of about 1 nm (55 metal atoms), a reasonably relevant model with respect to experiments (between ∼1 and 3.1 nm according to synthesis conditions [31,33,34]). The dissociative adsorption of a single H_2 molecule at the nanoparticle surface, as well as molec-

ular CO adsorption, will first be probed in order to spot potential favorable adsorption sites. The optimal coverage value of the system for higher coverage of hydrogen and CO will then be studied *via ab initio* thermodynamics calculations, a method intended to take into account realistic conditions of a molecular system in equilibrium with its environment. [26,35–38] (T, p) phase diagrams considering RuNPs in equilibrium with two distinct H_2 and CO sources were computed to provide an accurate description of the surface species under a wide range of experimental conditions. The main context of this study is the chemistry at the surface of colloidal nanoparticles, although the results obtained under ultra high vacuum conditions could also shed light on the structural and electronic properties of clusters produced by sputtering processes. [39–42] Using several indexes (d-band center, [6,43–45] crystal overlap hamilton population [46]) expanded in a local atomic basis set, a systematic analysis of the bond properties and of the electronic states will be done, in order to build a bridge between molecular coordination chemistry and the chemistry at the surface of RuNPs, following on from our previous work. [45] Several experimental results obtained these last years on RuNPs [31,33,47] will be revisited under this new perspective, but also in relation with the CO vibrations, which is a well-known probe of the metal-carbonyl interaction in organometallic chemistry. Finally, and thanks to the energy indexes and phase diagrams considered in this study, a possible reaction intermediate is proposed, as a possibly interesting piece in the complex Fischer-Tropsch puzzle.

2 Single H and CO adsorption on a RuNP

All properties were evaluated on an hcp-based Ru_{55} nanoparticle, shown in Figure 1a and described in detail in the "theoretical and experimental methods and models" section. The metallic character of this nanocluster can be clearly seen on the projected density of states (pDOS) of Ru_{55} which is reported in Figure 1b. Close to the Fermi energy, the total pDOS (in black) is dominated by the d component (in red). The d-band center for the 44 surface atoms and the 11 core atoms is calculated to be 2.6 eV and 3.6 eV. They will be compared later with the $Ru_{55}H_m(CO)_k$ compounds. Although the DOS and its decomposition over atomic orbitals are useful in identifying molecule-surface interactions and in quantifying the occupation of molecular orbitals or bands, they do not give a direct proof of the interaction between two species and of the nature of such interaction, i.e. bonding, non-bonding or anti-bonding. This can be obtained by analyzing the so-called crystal orbital overlap population (COOP [48]) or the crystal overlap hamilton population (COHP [46,49]), which has been prefered in the present work. Both functions provide an energy-resolved visualization of chemical bonding in molecules or in solids (more details are given in section 6). The COHP(ε) profile for the nearest neighbor Ru-Ru interactions in Ru_{55} is also reported in Figure 1b. It shows a bonding character of the states lying up to -5

eV, and then a slightly antibonding character of the occupied valence states close to the Fermi level, ε_F. This is reminiscent of the electronic structure in small organometallic clusters.[50] The integrated pCOHP (IpCOHP), a bond strength index, is found to be 45 kcal.mol^{-1}/Ru-Ru interaction.
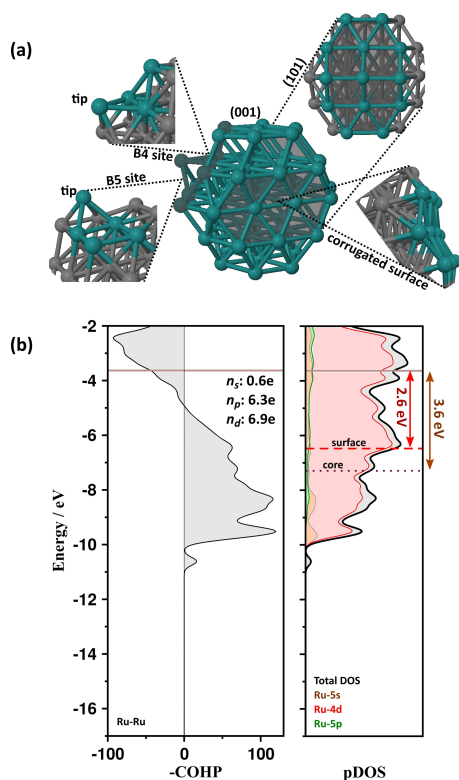
Fig. 1 (a) 55-atoms hcp-based RuNP and special sites at its surface; (b) Projected DOS and COHP analysis for the nearest neighbor interactions in the bare Ru$_{55}$nanocluster. The average occupation of the 5s (n_s), 4p (n_p) and 4d (n_d) bands are also reported, as well as the d-band center for surface Ru atoms (dashed red line) and for core Ru atoms (dotted black line) and the position of the Fermi level (brown horizontal line). The low-lying 4p-DOS does not appear in this energy range. pCOHP profiles are calculated for nearest neighbors only

Low coverage

In the colloidal context, RuNPs are usually prepared by hydrogenating at room temperature an organometallic precursor under a pressure of H$_2$ and in the presence of stabilizing ligands, such as the polyvinylpyrrolidone polymer (PVP), which offers steric protection, or the bisdiphenylphosphinobutane ligand (dppb), which offers both steric and electronic protection.[51] The nanoparticles are essentially covered with surface hydrides since H$_2$ easily adsorbs and dissociates at the surface. In order to probe the adsorption strength at various surface sites, we shall first consider the coordination of a single hydride at the nanoparticle surface. Many studies have shown the preference for a face-centered cu-

bic (fcc, μ_3) coordination of the H atom on the compact (0001) surface for Ru.[25,26,52] The Ru$_{55}$ nanoparticle considered in this study has a small (0001) facet on which the hydrogen atom can be coordinated, as can be seen on Figure 1a. But this site as well as the others many-fold sites on the studied nanoparticle are not exact μ and μ_3 sites as the M-H distances are not equal, as shown in Table S1. The adsorption energy obtained for μ coordination on the ruthenium nanoparticle is E_{ads} = -13.8 kcal.mol^{-1}, which is in the same order of magnitude as H adsorbed on (0001) surface at small H coverage and for single H adsorption on RuNP (-13.6 kcal.mol^{-1}).[23,53–55] In addition to this (0001)-like site, other surface sites have been investigated corresponding to η, μ or μ_3 bonding (Figure 2a). Detailed geometries of the considered H adsorption sites are given in Table S1 . Adsorption energies at the RuNP surface ranges from -5.6 to -14.9 kcal.mol^{-1} (see Table S2), with a clear preference for μ and μ_3 coordination. Adsorption energies are similar to or weaker than those calculated on the (0001) surface (-13.6 kcal.mol^{-1}). No particularly strong adsorption site has been found, unlike for differently shaped Ru$_{55}$ nanoparticle where a subsurface defect caused E_{ads} to drop to -27.3 kcal.mol^{-1}.[45] Since the adsorption of CO is non dissociative,[56] eq. 2 becomes $E_{ads}(CO) = E(M_{55}CO) - E(M_{55}) - E(CO)$ for a single carbon monoxide. Different coordination sites have been studied, all of them are reported in Table S3 and on Figure 2b. Detailed metal-CO distances are also given in Table S4. The 2^{OC} isomer differs from the others because in that case the CO is not coordinated via the carbon atom but by the oxygen atom. This leads to a weak adsorption energy (less than 4 kcal.mol^{-1}) and will not be furthermore considered. For the other structures, the coordination is done via the C atom in η, μ, μ_4, or both C and O atom for the (η, η^2) configurations. None of the RuNP/CO isomers retained μ^3 coordination. Comas-Vives et al.[55] showed that μ_3 adsorption can be found on the 0001 plane but with an adsorption energy of -40 kcal.mol^{-1}. In our case, adsorption energies range from -40.3 kcal.mol^{-1} to -52.7 kcal.mol^{-1}. This is quite a narrow range considering that adsorption energies up to -59 kcal.mol^{-1} have been found on Ru nanoparticles[45]. This is explained in the same way as for H adsorption: the high -59 kcal.mol^{-1} value as found on a very defective site with a subsurface vacancy leading to strong adsorption, which is not modelled on the present nanoparticle. Another site however emerges as a strong coordination site: the step-like sites, in the vicinity of the tip (see Figure 1). The most stable η (2^{CO}), μ (10^{CO}) and (η, η^2) (3^{CO}) coordination are found for RuNP/CO adsorbates involving at least one of the step-like site atom, as can be seen on Figure 2b. Overall, the preferred CO coordination modes are η and μ, but considering the narrow range of energies, all coordination modes have to be considered for higher coverages. Those results give references energies and adsorption trends for a single atom/molecule, i.e. for a very low coverage.
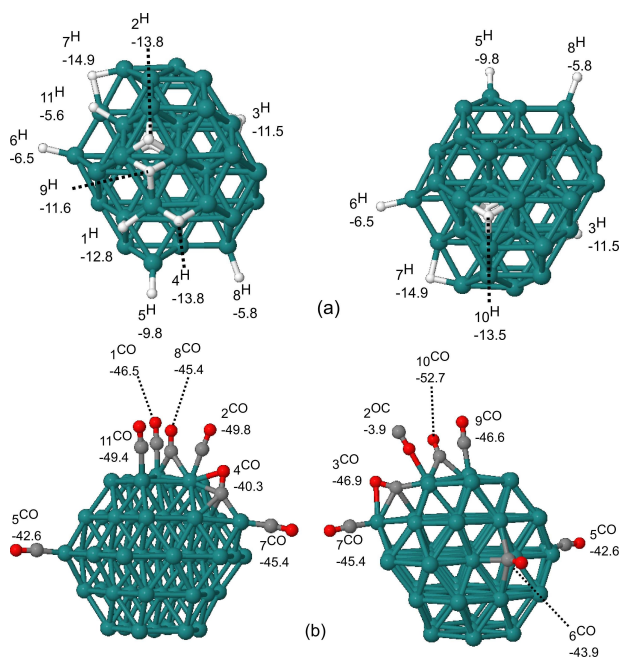
Fig. 2 Different adsorption sites at the Ru_{55} surface for H atom (a) and for CO (b) with different point of views. Each adsorbate*RuNP has been optimized separately. Adsorption energies are given in kcal.mol^{-1}

2.1 Multicarbonyl site at apex location

Metal atoms at apex sites of NPs are under coordinated. In the case of RuNPs, they are known to be possible adsorption sites for multicarbonyl ligands.[31] We computed the adsorption energies of one and two additional CO adsorbed on apex site starting from the 2^{CO} isomer (see Figure 2b). The resulting DFT-optimized geometries are given in Figure S2 . Whereas edge-bridging (μ) adsorption is preferred on the bare RuNP, the second addition on the same metal atom leads to a configuration with one atop CO and one bridging CO. The third addition leads to three μ-CO. Despite our attempts, we were unable to obtain the genuine multicarbonyl pattern, made of three terminal-CO coordinated to the same Ru atom. However, in contrast with standard edge-bridging CO, carbonyl ligands are not strictly perpendicular to the edge, owing to their mutual electronic repulsion. In terms of adsorption strength, adding a second CO on this site (2^{2CO}) does not affect the mean adsorption energy, it goes from -49.8 to -49.9 kcal.mol^{-1}. The adsorption of a third CO (2^{3CO}) on the same metal atom is less favorable than the atop grafting of carbonyl ligands on three different ruthenium atoms (-46.7 kcal.mol^{-1} vs. -51.8 kcal.mol^{-1}). The vibrational frequency of the CO stretching in 2^{2CO} is found to be 1898 cm^{-1}. Adding a second CO (2^{2CO}) only slightly affects the stretching of the atop CO which is down-shifted to 1883 cm^{-1}, whereas the second mode appears at 1785 cm^{-1}, as expected for bridging-CO. Finally, for 2^{3CO} the CO vibrates at 1875, 1795 and 1777 cm^{-1}.
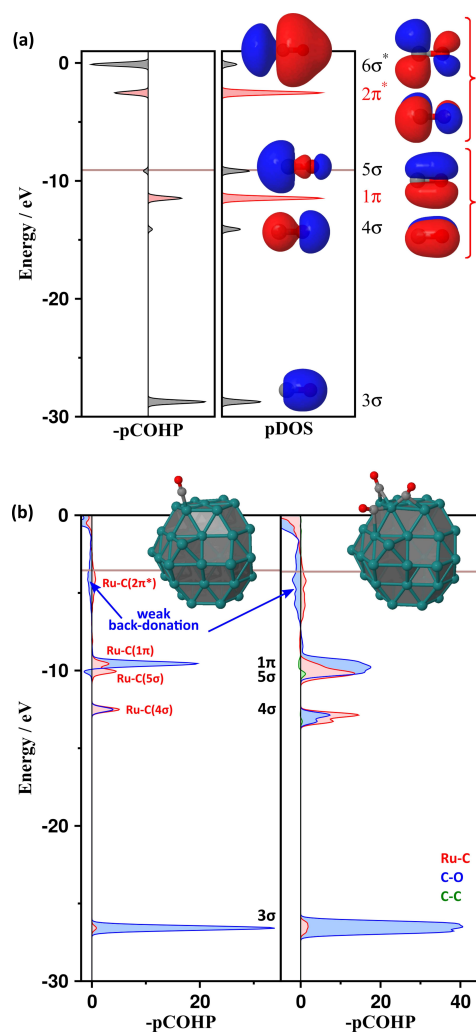
Fig. 3 (a) pCOHP and pDOS for CO (the energies and profiles were calculated with VASP: the σ DOS is projected onto the C and O $2s$ and $2p_z$ AOs, whereas the π DOS is projected onto the C and O $2p_x$ and $2p_y$ AOs. The Kohn-Sham MOs were computed within the PBE functional[57] with the Gaussian09 software[58], in a standard 6-31G** basis set[59]); (b) pCOHP for 2^{CO} and 2^{3CO} (The Ru-Ru interaction is not shown for the sake of clarity). pCOHP profiles are calculated for nearest neighbors only, with the exception of C-C interactions (2.5 Å < R_{C-C} < 3.2 Å). The z axis goes through the C and O atoms in 2^{CO} (see Figure S3 for a more detailed analyzis)

This case offers the opportunity to analyze the electronic feature of the carbonylation of a RuNP in terms of pDOS and pCOHP and to compare it with CO adsorption at transition metal surfaces.[60]. These functions for a free CO molecule, plotted in Figure 3a, provide reference data to be compared with the carbonylated RuNPs. Regarding chemisorption at surfaces, according to the Blyholder model,[61] the 5σ and $2\pi^*$ which correspond to the HOMO and the LUMO respectively, are the three most important

MOs. When CO is brought toward a metal surface, its grafting is ruled out by a σ-donation from the 5σ MO to the initially unoccupied d orbitals of the metal substrate and by a back-donation from the filled d orbitals of the metal to the $2\pi^*$ MO. In this model, the lower lying 1π, 4σ and 3σ MOs do not significantly interact with the band structure of the metal surface. Within DFT, the pCOHP analysis plotted in Figure 3b for $Ru_{55}(CO)$ shows that the 5σ MO is strongly stabilized due to the interaction with the substrate (a more detailed analysis is reported in Figure S3). As already pointed out by Scheffler and Stampfl[60] in the case of CO adsorption on the Ru(0001) surface, there is also a significant interaction between the 4σ MO and the delocalized $Ru-d_{z^2}$ states of the surface metal atoms. The OA-resolved pDOS plotted in Figure S3 also shows a resonance of $5s$ states at the 4σ position, not present in the bare Ru_{55} nanocluster. As expected, the 3σ MO does not play an important role in the CO-substrate bonding. On the contrary to the adsorption on the Ru(0001) surface, there is also a significant bonding interaction between the 1π MO and the $Ru-d_\pi$ states. The $2\pi^*$ MO, much more delocalized in $Ru_{55}(CO)$ than in a free CO, is mixing with the d_π component of the metal. As a result, there is a total of 0.7 electron in the $2\pi^*$ levels (whilst the 1π levels accommodate 4 electrons). IpCOHP is lower for the adsorbed CO than for the free CO, owing to the weak metal to ligand charge transfer from the Ru_{55} core to the $2\pi^*$ MO which is observed in the pCOHP profile (437 kcal.mol^{-1} vs. 454 kcal.mol^{-1}). Such one-electron derived energy must not be compared to the bond dissociation energy (BDE) of CO ($ca.$ 256 kcal.mol^{-1}) but it gives a valuable bond strength index which variation is expected to follow BDE variations. Overall, this analysis agrees in general with the Blyholder model, but the details of the bonding are somewhat more complicated. Regarding the multicarbonyl case, $Ru_{55}(CO)_3$, the bonding picture is essentially the same, with a broadening of the peaks, corresponding both to different coordination sites and to a small through space bonding/antibonding interaction between the carbonyl groups (green curve in Figure 3b, at $ca.$ -10eV).

2.2 High coverage. (T = 0 K, p = 0 Pa) limit

H chemisorption. The pressure (p_{H_2}) and temperature (T) of the reservoir of dihydrogen affects the coordination of H_2 at the catalyst surface and can lead to different stable coverages.[62] From a theoretical point of view, we shall see in the following that taking into account realistic experimental conditions in terms of pressure and temperature lead to drastically different optimal coverage values than DFT energies, which are the (T = 0 K, p = 0 Pa) limit. But it is interesting to first analyze the DFT adsorptions energies (eq. 2), in relation with the electronic features of the metal core.

We have studied the ruthenium nanoparticle with various H coverage values ranging from 0.02 ML to 2.5 ML. Several config-
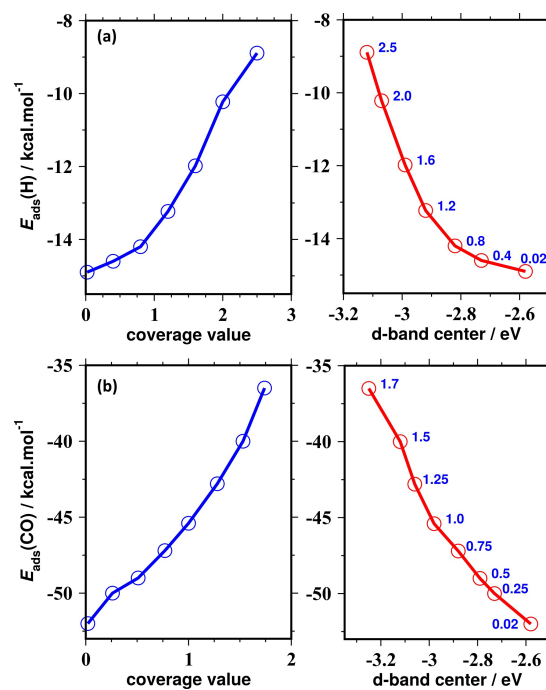
Fig. 4 Adsorption energies $E_{ads}(L)$ calculated with eq. 2 as a function of the coverage value (blue curves) and as a function of the d-band center, ε_d (red curves, coverage values are also indicated in blue). Top: hydrogenation; bottom: carbonylation

urations for the adsorbed H have been considered for each coverage value including some cases with subsurface hydrogen atoms, although hydrides are not expected to easily dissolve into ruthenium, even at very high pressure (see Figure S4a and Table S5). For the two lowest coverages, as hinted by calculations on a single H atom, a configuration with only edge-bridging and face-capping H atoms is found to be the most stable, but as the coverage increases, η coordination modes appear. For 2.5 ML, non dissociated η^2-H_2 can also be found on the surface, possibly due to a weaker back bonding from the metal to the σ^* MO of H_2 at such high coverage. The dissociative adsorption energy per hydride is reported in Figure 4a as a function of the coverage value. The higher the coverage value, the weaker the adsorption strength. In other words, at the (T = 0 K, p = 0Pa) limit, the optimal coverage is very far from a saturation of the surface. The second plot in Figure 4a shows the dependence of $E_{ads}(H)$ as a function of the d-band center of surface metal atoms, $\varepsilon_{d,s}$: the lower the d-band center of hydrogenated Ru_{55} clusters, the weaker the average adsorption energy, as expected. Moreover, the adsorption energy decreases faster than ε_d, owing to strong steric interactions between H atoms at high coverage. In summary, adsorption energies are strongly related to the intrinsic electronic properties of the metal core and to steric effects, and cannot account for the experimental optimal coverage which lies between 1.3 and 2.0 H

per surface ruthenium atom.[55,63]

pDOS(ε) and pCOHP(ε) of Ru$_{55}$H$_{70}$ (1.6 ML) and Ru$_{55}$H$_{110}$ (2.5 ML) are plotted in Figure 5. In both cases, the d-band center of the metal core, ε_d, is stabilized with respect to the bare Ru$_{55}$ NP by 0.4-0.5 eV, due to bonding interactions with surface ligands that widens the d band (in red on the pDOS plot, to be compared with Figure 1b). As it is already the case for Ru$_{55}$, the highest Ru states have an antibonding character which slightly weakens the Ru-Ru bond strength, whereas pCOHP$(\mathrm{Ru-H}, \varepsilon)$ is always positive below the Fermi level. Regarding Ru$_{55}$H$_{110}$, the main difference with respect to Ru$_{55}$H$_{70}$ is the appearance of states lying between -13 eV and -12 eV. It is related to the coordination of undissociated dihydrogen molecules (green curve in the pCOHP plot), which are the result of the local geometry optimization. They were not introduced in the initial geometry to be optimized, but a high coverage of the metal surface lowers the M$\to\sigma^*$ back-bonding responsible for H$_2$ dissociation. Given that dihydrogen complexes M(η^2-H-H) have proven to be very important in the chemistry of ruthenium, such σ complexes being able to act as reaction intermediates, this is an interesting result. Unfortunately, it will be shown later in this article that such high coverage is unlikely to be observed. But this results gives an interesting indication that co-adsorbed species able to mobilize the d AOs of the RuNP surface could favor the sideways coordination of H$_2$.

CO chemisorption. The CO on the Ru(0001) adsorption system has been widely studied. The adsorption energy varies with coverage from 38 to 42 kcal.mol^{-1} in the 0.33 ML to $\sim$0 ML coverage regime.[64,65] According to investigations performed in the temperature range 80-400 K with IR reflection-absorption spectroscopy, the preferred site is the atop site for coverages up to 0.33 ML and then reduces to 29 kcal.mol^{-1} at high coverage.[66] CO adsorption and dissociation on ruthenium surfaces has also been investigated quite extensively at the DFT level, often in the context of the Fischer-Tropsch reaction.[5,16,19,29,30,67,68] The case of RuNPs stabilized only by carbonyl ligands is now going to be considered. On the experimental side we took as reference an article published by the Philippot and Chaudret groups.[33] In this work, CO adsorption has been used as a probe to identify the available surface sites. Their location on 1.7 nm RuNPs@PVP and 2.0 nm RuNPs/dppb and their characterization has been achieved by infrared and solid state NMR spectroscopy. After exposure of the samples under 0.5 bar of CO, titration experiments revealed the absence of remaining hydrides on the surface, whereas the ^{13}C MAS NMR spectra of these RuNPs exhibit a strong signal near 250 ppm assigned to bridging CO ligands with an additional peak near 190 ppm that may arise from multicarbonyl sites at apex locations of the particle.[31] These results are now going to be analyzed in terms of DFT energies and wavefunctions of several Ru$_{55}$(CO)n NPs. Again, several coverage values were considered ranging from 0.02 ML to 1.70 ML (see Figure S4b and Table S6).

The average adsorption energy, E_{ads}(CO), is reported in Figure 4b as a function of coverage. CO is strongly bound to the surface, from -50 kcal.mol^{-1} for low coverage values, up to *ca.* -36 kcal.mol^{-1} only for 1.7 ML. The average adsorption energy calculated for 0.25 ML (Ru$_{55}$(CO)$_{11}$) is slightly lower than the adsorption energy of a single CO group (section 2) as expected from the lack of steric discomfort of the 11 CO and from the similar ε_d value (-2.73 eV *vs.* -2.58 eV). As previously observed with H, there is a nice correlation between adsorption energies and the d-band center of the metal core (red plots in Figure 4b). These adsorption energies involve that co-adsorption of H and CO in similar amounts will not be easy to achieve under experimental conditions, since CO is more strongly coordinated than H by a factor of 4 to 3 according to coverage.

pDOS(ε) and pCOHP(ε) for Ru$_{55}$(CO)$_{66}$ (1.5 ML) are plotted in Figure 5c. As already analyzed in section 2.1, the bonding picture is less simple than the usual Blyholder model, which relies only on a joint 5σ donation and 2π^* back-donation.[61] Both the 4σ and the 5σ MOs interact with the surface, whereas a substantial back-donation from the RuNP metal core to the 2π^* MOs arises in addition to the interaction between the 1π MOs and the d_π states of the substrate. The pCOHP(ε) curve is strongly reminiscent of the multicarbonyl pCOHP(ε) curve plot in Figure 3b, with a broad 4σ band and two broad 1π and 5σ bands. Since the 5σ MO is mainly non-bonding between C and O, it is not responsible for the CO-bonding (blue curve) between -13 eV and -10 eV, which can be safely assigned to the 1π MOs. The splitting of the 1π curve is due to a bonding/antibonding interaction between the carbon (green curve) and oxygen atoms of the carbonyl bound to the same Ru atom, the so-called multicarbonyl ligands. With respect to what is usually analyzed on close-packed surfaces,[60,69] this is a novel electronic signature of metal NPs saturated with atop and edge-bridging CO ligands.

2.3 Phase diagrams

Hydrogen chemisorption. Several geometry configurations have been considered for each coverage value,[70] Their total energy, the number of hydrides per type of coordination, the standard Ru-H vibrational frequencies and the surface area A_{NP} (eq. 8) are given as the input of the *aithermo* code, which identifies which is the most stable configuration for each temperature (T) and pressure ($p_{\mathrm{H_2}}$) in a specified range of temperature and pressure. Figure 6a shows the resulting ($T, p_{\mathrm{H_2}}$) phase diagram, whereas $\Delta_a G(T)$ for $p_{\mathrm{H_2}} = 1$ bar and $p_{\mathrm{H_2}} = 10^{-7}$ bar, characteristic of standard nanoparticle synthesis *via* the organometallic route and *via* the molecular physics way respectively, are reported in Figures 6b and 6c. The ($T, p_{\mathrm{H_2}}$) phase diagram obtained without taking into account the Ru-H vibrations, *i.e.* the zero point energy (ZPE), is reported in the SI (Figure S5). As mentioned in a previous study,[26] whereas it does not qualitatively change the
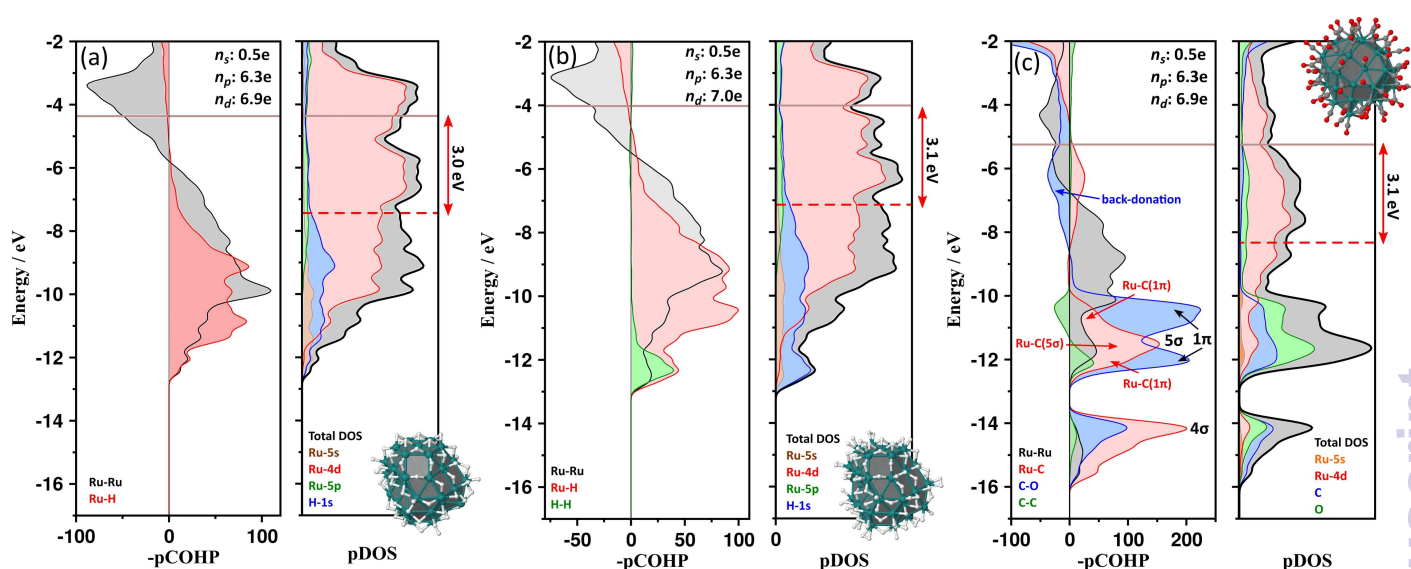
Fig. 5 Projected DOS and COHP profiles for (a) $Ru_{55}H_{70}$ (1.6 ML), (b) $Ru_{55}H_{110}$ (2.5 ML) and (c) $Ru_{55}(CO)_{66}$ (1.5 ML). Conventions are the same as in Figures 1 and 3

diagrams, each surface composition being significantly shifted to higher T and lower p.

Using the same methodology, we showed earlier that coverages above 1 ML on Ru(0001) are not the most stable at any considered values in the (T,p) domain, in agreement with experimental data.[26] Titration experiments achieved on 1.5 nm spherical hcp RuNPs@PVP showed that they can accommodate at least 1.3 hydride per surface ruthenium atom.[63] Other experiments on 1.6 nm silica supported RuNPs estimate that 2.0 hydrides per surface atom can be found.[55] On the theoretical side, the phase diagram calculated for Ru_{55} evidence six stability domains ranging from 1.6 H by surface atom to the bare surface when the temperature increases. For 1.2 ML, there is a transition between two different configurations with the same coverage value for high temperatures: from 1.2 ML_1 to 1.2 ML_2 three hydrogen atoms that are in μ_3 coordination switch to μ. In typical medium vacuum pressure ($p = 10^{-7}$ bar), the transitions between the different coverages occur at 168 K for 1.6 ML to 1.2 ML_1, at 275 K for 1.2 ML_1 to 0.8 ML, 337 K for 0.8 ML to 0.4 ML and 368 K for 0.4 ML to the bare nanoparticle. Those low temperatures evidence the fact that under these conditions no, or very little, H adsorption is expected at room temperature and above. Increasing the pressure at 1 bar of hydrogen dramatically changes the stability of the different coverages. For instance, the bare nanoparticle is now the most stable only above 755 K; the nanoparticle with 0.4 ML between 755 K and 705 K; 0.8 ML between 705 K and 542 K; 1.2 ML_1 between 542 K and 347 K and 1.6 ML under 347 K. It is worth noting that none of these external conditions favor isomers with subsurface hydrogen atoms, even high pressures. Unlike the surfaces, cover-

age ratios above 1 ML are favored in most of temperature range for the two pressures, and 1.6 ML is the most stable coverage under standard conditions, in agreement with the experimental value of at least 1.3 hydride per surface ruthenium atom.[31,63]

CO chemisorption. *Ab initio* thermodynamic phase diagrams have also been calculated in order to estimate the optimal coverage of RuNPs by carbon monoxide. Figure 6d shows the *ab initio* thermodynamics phase diagram with (eq. 8) vibrational contribution from the adsorbed CO. $\Delta_a G(T)$ is plotted for $p = 1$ bar in Figure 6e and for $p = 10^{-7}$ bar in Figure 6f. The (T, p_{CO}) phase diagram without ZPE corrections is reported in Figure S6. In contrast with H, ZPE corrections have little influence on $\Delta_a G$.

The diminution of adsorbed CO ligands as the temperature increases is less drastic than calculated for hydrogen. Since CO ligands adsorb more strongly than H atoms, the bare RuNP is not expected to be obtained in the [0, 1000 K] range under 1 bar of pressure. At $p = 10^{-7}$ bar, the most stable structure has 1.75 CO per surface atom from 0 K to 96 K ; 1.5 between 96 K and 305 K ; 1.25 between 305 K and 405 K ; 1.0 between 405 K and 480 K, 0.75 between 480 K and 534 K ; 0.5 between 534 K and 607 K ; 0.25 between 607 K and 632 K, and bare at higher temperature. At $p = 1$ bar, the stability of structure covered with CO is even more important as there is no temperature in the considered 0-1000 K range for which the bare nanoparticle is the most stable. Between 1000 K and 918 K, the most stable is 0.5 ML; between 918 K and 825 K it is 0.75 ML; between 825 K and 682 K 1.0 ML; between 682 K and 513 K 1.25 ML; between 513 K and 164 K 1.50 ML and under 164 K it is 1.75 ML. Therefore, under standard conditions, the most stable coverage is 1.50 ML
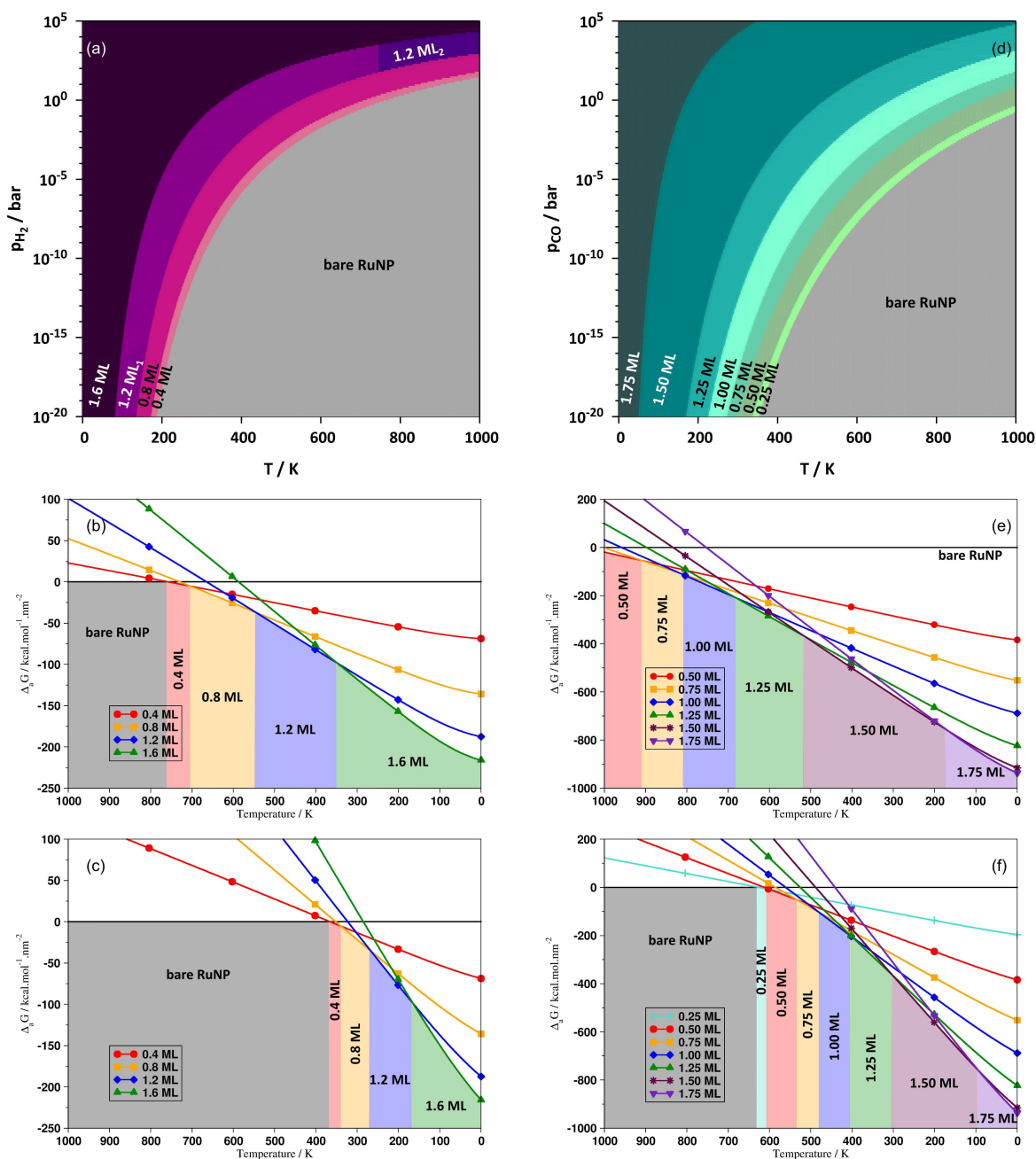
Fig. 6 (a) (T, p_{H_2}) phase diagram for H_2 adsorption on the 55-atoms RuNP; variation of Gibbs free energy of adsorption of H_2 on the 55-atoms RuNP, including vibrational contributions, as a function of temperature for $p_{H_2} = 1$ bar (b) and $p_{H_2} = 10^{-7}$ bar (c). (d) (T, p_{CO}) phase diagram for CO adsorption on the 55-atoms RuNP; variation of Gibbs free energy of adsorption of CO on the 55-atoms RuNP, including vibrational contributions, as a function of temperature for $p_{H_2} = 1$ bar (e) and $p_{H_2} = 10^{-7}$ bar (f). The (T, p_{H_2}) and (T, p_{CO}) phase diagrams obtained without taking into account ZPE corrections are reported in the SI, see Figures S5 and S6)

$(Ru_{55}(CO)_{66})$. This coverage corresponds to CO adsorbed preferably in μ coordination, with also η adsorption favored (34 μ and 25 η). Due to the irregularities of the surface, a few number of

face-capping μ_3-CO also lie on it, and one (η, η^2)-CO is coordinated in the vicinity of the tip. As expected from experiments,[31] multicarbonyl are observed at apex sites with the in-between μ-

and η- coordination pattern described earlier. This trend is observed for all coverage ratios above 1.00 ML. For 1 ML coverage and under, the μ/η ratio is way higher, and structures with the higher number of μ-coordinated CO are the most stable according to $\Delta_a G(\text{T})$. For coverage ratios under 0.5 ML, multicarbonyl coordination is not favorable enough to overcome the μ preference.

3 H and CO co-adsorption on a RuNP

3.1 Experimental context and ($T = 0$ K, $p = 0$ Pa) study

Let us first draw up an overview of the theoretical knowledge on the Ru(0001) surface. According to DFT calculations, CO adsorption on H covered Ru(0001) surface is an activated process, with the lowest barrier being 6 kcal.mol^{-1}, *i.e.* very easy to overcome at r.t.[27] Experiments performed in the same study revealed an additional non-activated reaction channel, due to CO adsorption at defects, and possibly due to the motion of H-atoms within the H overlayer. According to DFT, at high hydrogen coverage (1ML) CO adsorbs preferentially atop. DFT calculations also showed that for the H co-adsorption with CO, the lateral interactions are repulsive, and H and CO prefer to segregate rather than to form mixed structures.[23] In addition, this study showed that CO is little influenced by co-adsorption, except when 1 ML of atomic hydrogen is pre-adsorbed. In that case, the adsorption strongly decreases: it was found to be -9 kcal.mol^{-1} (atop-CO with four fcc-H), -12 kcal.mol^{-1} (atop-CO with four hcp-H), +3 kcal.mol^{-1} (hcp-CO with four fcc-H), and less than +3 kcal.mol^{-1} (fcc-CO with four H in hcp sites). Within the employed functional (PW91), these numbers have to be compared to the adsorption of CO (43 kcal.mol^{-1}) and to the simultaneous adsorption of one CO ligand and one H atom, which yields two close adsorption energies according to their respective bonding: 43 kcal.mol^{-1} (atop-CO and fcc-H) and 42 kcal.mol^{-1} (hcp-CO and fcc-H).

Geometries. We have considered several combinations of H and CO coverages, which are summarized in Figure 1 and in Figure S7 as well as in Table S7. In those covered RuNPs, the surface composition ranges from 0.02 ML to 1.23 ML for hydrogen and from 0.02 ML to 1.5 ML for CO. Several starting configurations were considered for each composition, with η-CO or μ-CO or μ_3-CO only, or with a combination of these three types of coordination in different proportions, the hydrogen being mostly coordinated in μ or μ_3 sites, with in some cases a few number of atop-H. Regardless of the starting geometry, the optimization leads to mainly μ-H and μ_3-H with some atop H when the total number of ligands increases, whereas CO is mostly atop and edge-bridging coordinated, with a very few number of threefold CO and an overall preference for μ-CO. As already observed with $Ru_{55}(CO)_n$ NPs, multicarbonyl sites appear at apex and edge positions when the CO coverage increases. It is worth noting as well that one or two (η, η^2)-CO, *i.e.* carbonyl ligands lying parallel to the surface, arise

in the vicinity of the surface tip. On such a non-symmetric and corrugated NP, geometry optimizations of μ-CO-covered RuNPs often lead to a small amount of face-capping CO, as already observed in $Ru_{55}(CO)_n$ compounds. For instance, a starting geometry with 0.5 ML H and 0.5 ML μ-CO relaxes to a configuration in which more than half of the initial μ-CO has switched to either η or μ_3 coordination. For a same H coverage value, increasing the amount of adsorbed CO leads to a higher number of η-coordinated CO, but the preference for μ-CO is still observed as, even for 0.25 ML H:1.50 ML CO (*i.e.* $Ru_{55}H_{11}(CO)_{66}$) the number of μ-CO exceeds the η-coordinated ones. The same preference is also observed when increasing the quantity of adsorbed hydrogen for a constant CO coverage. The opposite can be said on μ_3-CO, as their number is quite constant and low, so their proportion lessens when the number of surface ligands raises. Overall, optimal geometries are characterized by coverages with a high amount of μ-CO ligands, a lesser amount of η-CO, and a very few number of μ_3-CO (see Table S7 for a description of the coordination modes of carbonyl compounds for each considered surface coverage).

Adsorption energies. Let's move on now to adsorption energies. As already recalled, in the colloidal context we essentially refer to in this article,[51] the synthesis of RuNPs is performed by hydrogenating at r.t. an organometallic precursor (p_{H_2}: 3 bar) in the presence of an ancillary ligand. Using PVP, the surface is fully covered with H atoms only. According to our calculations, the H_2 average dissociative adsorption energies is -9.3 kcal.mol^{-1} for 1.6 ML on Ru_{55}. Addition of CO to H-covered RuNPs can then be done. Hydrides and carbonyl ligands compete for sites on the surface, with a strong -40 kcal.mol^{-1} average adsorption energy for 1.5 ML CO on a bare Ru_{55} NP, in line with a carbonyl-poisoning of the catalyst. Recently, addition of CO on a solid sample of hydrogenated Ru@PVP NPs was monitored by ^{13}C solid-state NMR spectroscopy.[33] It showed that upon allowing the system to react for a long time period, coordination of CO occurs first in a bridging mode and then in a terminal one. Besides, in the same article, the authors demonstrated that although the surface of Ru@PVP and Ru/dppb accommodates between 1.2 and 1.6 hydrides per surface Ru atoms, no hydride could be detected after treating these NPs with CO at r.t. The catalytic hydrogenation of styrene under mild conditions was also evaluated. Whereas full conversion to ethylbenzene and ethylcyclohexane was observed on RuNP@PVP and RuNP/dppb, almost no conversion was observed on the same NPs saturated with CO, even at 80°C and after 60 hours, probably because a CO-saturated surface impedes the coordination of styrene. It seems however possible to obtain nanoparticles with both H and CO lying on the surface, by CO_2 reduction by H_2 at 120°C. As a matter of fact, the resulting NPs were proved to be reactive towards styrene, in contrast with the RuNP/CO@PVP and RuNP/CO/dppb. According to our DFT

calculations, the average adsorption energy of 11 CO groups on an H-saturated RuNP ($Ru_{55}H_{70}(CO)_{11}$, 1.60 ML H:0.25 ML CO) is -41 kcal.mol^{-1}, *i.e.* it is very favorable according to thermodynamics. In order to shed light on the poisoning effect of CO, let us consider for example the energy yield of the exchange reaction $Ru_{55}H_{70}(CO)_{11} + 32\,CO \longrightarrow Ru_{55}H_{22}(CO)_{43} + 24\,H_2$. The desorption of 24 H_2 molecules and the adsorption of 32 additional carbonyl compounds is exothermic by 18 kcal.mol^{-1} per CO ligand. The further replacement of 22 hydrides by the same number of carbonyl ligands is exothermic by 20 kcal.mol^{-1} per CO ligand. These results clearly show that without the help of a high pressure of H_2 with respect to CO, hydrides are not expected to be present on the surface of RuNPs. The influence of (T, p_{CO}, p_{H_2}) on the possible co-existence on both species on RuNPs in equilibrium with gas-phase H_2 and CO will be examined in a forthcoming section.
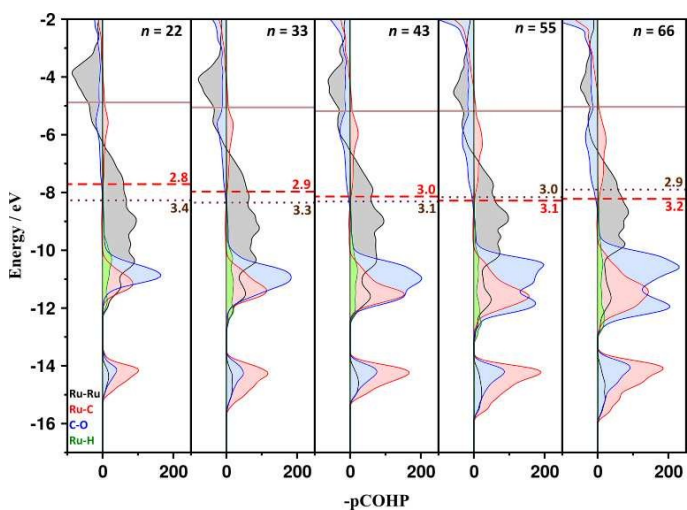
Fig. 7 pCOHP profile for $Ru_{55}H_{11}(CO)_n$. *d*-band center levels are also given for surface Ru atoms (dashed red lines) and for core Ru atoms (dotted maroon lines). The d-band center energies, ε_d (in eV. Red: surface atoms, maroon: core atoms), are calculated with respect to the Fermi level

Electronic features and practical consequences. But prior to this, the pCOHP profiles and *d*-band centers indexes are now going to be analyzed when a moderately hydrogenated RuNP, $Ru_{55}H_{11}(CO)_n$, is progressively covered with CO ligands ($n = 22 - 66$). The results are summarized in Figure 7. They all exhibit the same features: a bonding Ru-Ru interaction, which turns slightly antibonding below the Fermi energy; two Ru-C patterns, centered at -11 eV and -14.5 eV, corresponding to the $4\sigma_{CO}$ and $5\sigma_{CO}$ donation to the metal surface; one $1\pi_{CO}$ band at low CO coverage, also centered at -11 eV, which is split into two components when the coverage increases, as already discussed previously; a wide antibonding metal-to-$2\pi^*$ band just below the Fermi

energy, which intensity is proportional to the number CO lying on the surface; a large bonding Ru-H pattern centered at -11 eV, which surface is significantly smaller than the Ru-C bands owing to the higher number of CO ligands and to the stronger Ru-C bond strength. In the case of $Ru_{55}H_{11}(CO)_{22}$, IpCOHP(Ru-C) is found to be 102 kcal.mol^{-1} per Ru-C bond, whereas IpCOHP(Ru-H) is found to be 48 kcal.mol^{-1} per Ru-H bond. Regarding the center of mass of the occupied *d*-band, let us first recall that the *d*-band center of the surface atoms ($\varepsilon_{d,s}$) and of the core atoms ($\varepsilon_{d,c}$) of the naked Ru_{55} nanocluster lie at 2.6 eV and 3.6 eV below the Fermi level (Figure 1b). Upon going to $Ru_{55}H_{11}(CO)_{22}$, the bonding interaction between the substrate and the CO and H ligands involves a stabilization of $\varepsilon_{d,s}$. A destabilization of $\varepsilon_{d,c}$ is observed as well, which can interpreted as a new involvement of a fraction of the *d* electrons of the surface atoms in the bonding with surface species, instead of the bonding with the core metal atoms. $\varepsilon_{d,s}$ and $\varepsilon_{d,c}$ energies even cross beyond $Ru_{55}H_{11}(CO)_{43}$, in line with an electronic saturation of the metal substrate by surface species. The *d* electrons of surface atoms are more and more involved with the coordination of carbonyl groups and hydrides. As a consequence, the bonding interaction between the *d* AOS of the core atoms and of the surface atoms, which is at the basis of the strong stabilization of $\varepsilon_{d,c}$ in less saturated RuNPs, is reduced. By the way, the IpCOHP indexes follows this trend: IpCOHP between surface and core atoms in these $Ru_{55}H_{11}(CO)_n$ compounds is found to be 1.86 eV for n=22 and 1.75 eV for n=66; in the mean time, the interaction between core atoms is slightly strengthened (1.60 eV *vs.* 1.70 eV), whereas the interaction between surface atoms is lowered (1.93 eV *vs.* 1.53 eV).

The weakening of the surface-surface and core-surface interactions, related to the increase of $\varepsilon_{d,c}$ toward the Fermi energy suggests that small surface atoms may migrate under the surface. It is in qualitative agreement with previously calculated diffusion barriers of H atoms from the fcc site toward the closest octahedral site (os), which were found to be high on Ru(0001) surface with a 1/4 ML surface hydrides coverage (25 kcal.mol^{-1}), whereas an increase of the hydrogen coverage above 1 ML reduced this diffusion barrier (18 kcal.mol^{-1}).[26] In both cases, the reaction was found to be endothermic, by 22 kcal.mol^{-1} and 7 kcal.mol^{-1} respectively. As expected from the ε_d and IpCOHP indexes, the fcc site-os site diffusion barrier in $Ru_{55}H_{11}(CO)_{66}$, drops to 11 kcal.mol^{-1} (see Figure S8), but the reaction remains endothermic, by less than 4 kcal.mol^{-1}. Unfortunately, we shall see in section 3.3 that a surface saturated with CO ligands, with additional 1/4 ML surface hydrides is not expected to be obtained under FTS conditions. Nevertheless, this result confirms that the $\varepsilon_{d,c}$, $\varepsilon_{d,s}$ and IpCOHP indexes may be related to some interesting surface and subsurface adsorption features. The interesting summary of this study is that, in the limit of saturated surfaces, the interactions between surface metal atoms weaken. To some extent, this

may facilitate the migration of small species toward the sublayer. In the mean time, subsurface metal atoms could compensate the decrease of the first-layer/sublayer interaction, by making new bonds with subsurface species.

3.2 IR spectra
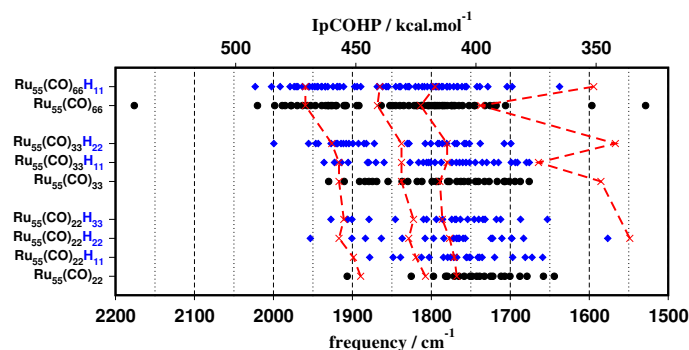
Fig. 8 Calculated CO stretching frequencies as function of the CO and H coverage. The averaged IpCOHP indexes for CO bonds are also reported (red dashed line, from left to right: η-CO, μ-CO, μ_3-CO , (η,η^2)-CO)

The vibrational frequencies for all the CO at the RuNP surface were calculated for selected cases. The computed vibrational CO frequencies according to the coverage are shown on Figure 8. We shall first comment the purely carbonylated cases that will be compared to recent DFT calculations on similar compounds which were recently published as additional support to observed frequencies for supported RuNPs.[55] A discrepancy between the IR spectra of supported RuNPs[55] and colloidal RuNPs[33] deserves additional comments. In the latter case, to which we have often compared our results from the beginning of this paper, a series of IR spectra of the Ru@PVP nanoparticles was recorded in the region of CO absorptions for different times of reaction. The spectrum initially shows a single absorption at 1945 cm^{-1}, assigned to bridging carbonyl ligands, which after 12 h at room temperature transforms into a very broad and more complex band centered at 1970 cm^{-1} resulting from multiple individual bands which can be either terminal or bridging CO ligands. In the case of supported RuNPs, a distribution of bands is obtained, where the band which exhibits the highest relative intensity is centered at 2046 cm^{-1} instead of 1945 or 1970 cm^{-1}. Our simulated spectrum for the 1.5 ML case (Ru$_{55}$(CO)$_{66}$) is very similar to a recently calculated DFT spectrum[55], apart that it is downshifted by *ca.* 100 cm^{-1}, probably owing to the different functionals used in both studies (PBE *vs.* revPBE) and to a stronger back-donation with the PBE functional which weakens the CO bond strength. Owing to the complexity of the experimental spectra, making a secure assignation of the experimental peaks is not easy, since standard DFT methods are not able to compute reliable intensities of the normal modes

of vibration. But overall, the IR frequencies of our Ru$_{55}$(CO)$_{66}$ structure, which is essentially intended to describe a stable equilibrium structure under CO exposure, *i.e.* with a mixture of bonding situations, agree rather well with the broad band recorded after 12h at r.t. for RuNPs@PVP. Although the theoretical spectrum is slightly downshifted with respect to any of the aforementioned experiments, it provides a reliable hierarchy of frequencies, ranging in our case from 1700 cm^{-1} to 2000 cm^{-1}: two frequencies below 1600 cm^{-1} correspond to CO adsorbed on step, a pre-dissociated state unlikely to be observed in a large amount on small NPs; the scarce μ_3-CO lying on the surface are responsible for the lowest part of the simulated spectrum; the highest part of the spectrum is related to terminal CO; the bridging CO lie in between. The high frequency calculated at 2176 cm^{-1} is a strongly delocalized mode that involves carbonyl ligands mainly located at apexes and edges. On going from Ru$_{55}$(CO)$_{22}$ to Ru$_{55}$(CO)$_{66}$ the CO stretching mode shifts to higher frequency, in agreement both with the recent experiments made on RuNPs[33,55] and with the knowledge in surface science.[71] This trend follows the average IpCOHP value, which is respectively 418, 430 and 449 kcal.mol^{-1} for Ru$_{55}$(CO)$_{22}$, Ru$_{55}$(CO)$_{33}$ and Ru$_{55}$(CO)$_{66}$. This increase of the CO bond strength is also related to the increase of the *d*-band center value of the surface atoms as the coverage increases (2.93, 2.98 and 3.02 eV with respect to E_F). ε_d seems to indicate that the *d*-orbitals and their electrons are less and less available for subsequent back-donation to the $2\pi^*$ MOs.

Let us now move on to some RuNPs both hydrogenated and carbonylated. In all the cases reported in Figure 8, a significant amount of hydrogen atoms is needed to shift the calculated spectrum to higher frequencies, by *ca.* 50 to 100 cm^{-1}. Again, this result correlates rather well with the IpCOHP value as well as with ε_d. Ru$_{55}$(CO)$_{22}$H$_n$, with n=0, 11, 22 and 33: IpCOHP = 418, 423, 421 and 428 kcal.mol^{-1}, ε_d = 2.93, 2.94, 2.98 and 3.0 eV Ru$_{55}$(CO)$_{33}$H$_n$, with n=0, 11, 22: IpCOHP = 430, 430 and 441 kcal.mol^{-1}, ε_d = 2.98, 2.99 and 3.02 eV; Ru$_{55}$(CO)$_{33}$H$_n$, with n=0, 11: IpCOHP = 449 and 450 kcal.mol^{-1}, ε_d = 2.98 and 3.12 eV. The IpCOHP values are reported on Figure 8 (red dashed lines) in order to better visualize their correlation with the frequencies shift which affects all CO coordination modes. Again, this underlines that such simple criteria, built on a one-electron picture, are quite powerful and that they bring a full set of valuable information and analysis in addition to the numbers delivered in computational chemistry.

3.3 Phase diagrams
In the Fischer-Tropsch process, the catalyst is exposed to a mixed atmosphere of gaseous H$_2$ and CO. The previous phase diagrams account for the adsorption of a single kind of ligand at the RuNP surface. Including a second one in the *ab initio* thermodynamics allows to establish 3D phase diagrams as a function of H$_2$ pres-
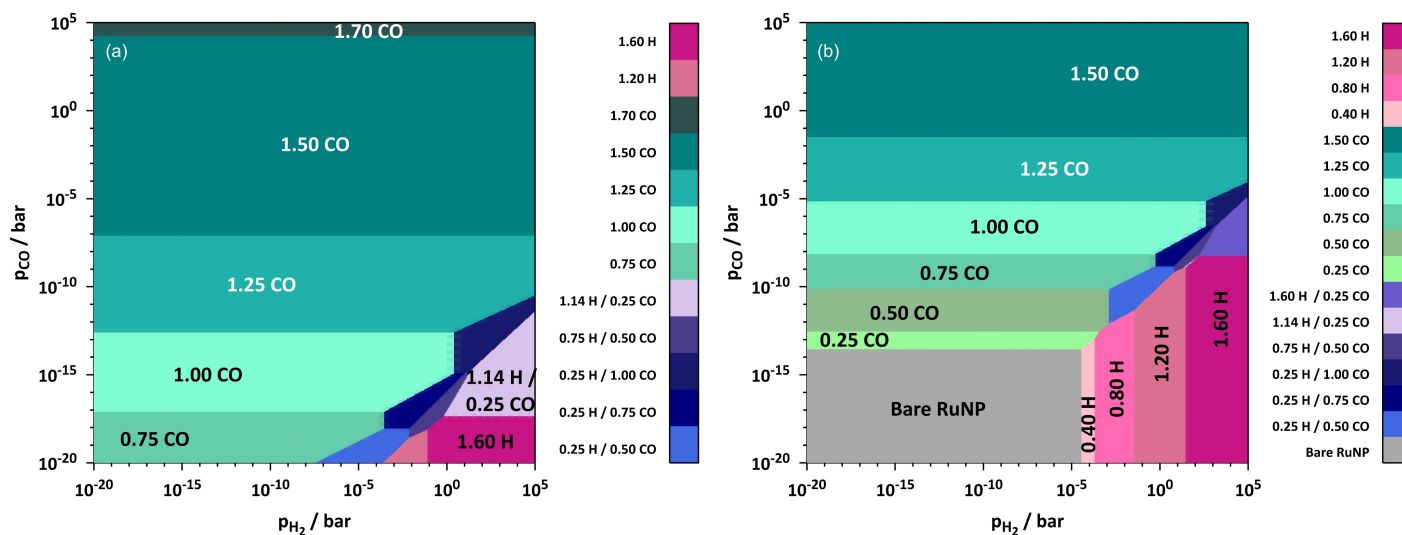
Fig. 9 Phase diagram for H_2 and CO adsorption on RuNP at 300 K (a) and 450 K (b). Horizontal domains corresponds to only CO adsorbed domains; vertical ones to only H adsorbed; oblique zones are domains in which H and CO are co adsorbed

sure (p_{H_2}), CO pressure (p_{CO}) and temperature. By fixing the temperature, 2D phase diagrams can be plotted as a function of the respective pressure of the ligands. Figure 9 shows two (p_{H_2}, p_{CO}) phase diagrams calculated at $T = 300$ K and $T = 450$ K, which result from the DFT energies of all the structures in Figures S4 and S7. Again, even if several compositions and configurations have been considered, only the most stable ones according to $\Delta_a G$ are reported in Figure 9.

The ab initio thermodynamics phase diagram calculated at 300 K is divided in three domains. In the largest one, only CO is adsorbed at the RuNP surface. It ranges from UHV-like pressures of CO and H to standard pressures and beyond. In order to have hydrides only lying on the surface, two separated sources should be set up, with p_{CO} kept under 10^{-17} bar and p_{H_2} set to at least 10^{-3} bar. Such conditions lead to a specific H-zone in the phase diagram, with various compositions. Finally, an oblique domain is observed for which H and CO can be coadsorbed on RuNPs. In order to reach it p_{CO} has to be kept below 10^{-11} bar, far below the usually employed $p_{CO} = 1$ bar in the FTS conditions. For (p_{H_2},p_{CO}) = (1 bar, 1 bar), we find that the most stable coverage is 1.5 CO ML, without any hydrides. Increasing the temperature to 450 K, shifts the three domains in the diagram. Below (p_{H_2},p_{CO}) = ($\sim 10^{-5}$ bar, $\sim 10^{-14}$ bar) CO and H do not adsorb at the RuNP surface. Increasing p_{CO} above this threshold results in CO-only covered RuNPs, and in the same way, p_{H_2} higher than 10^{-5} starts to yield covered RuNPs provided that p_{CO} is low enough. The H/CO co-adsorption domains is much reduced as compared to the one at 300 K but is also closer to standard experimental conditions as it includes pressures going from (p_{H_2},p_{CO}) = (10^{-3} bar, 10^{-12} bar) to (p_{H_2},p_{CO}) = (10^5 bar, 10^{-4} bar). Nev-

ertheless, at (p_{H_2},p_{CO}) = (1 bar, 1 bar), the most stable coverage is still 1.5 CO ML.

In both cases, H-only and CO-only adsorbed coverages follow the same coordination trends as for single adsorption. The most stable co-adsorbed structures are the same for the two considered temperatures. In each case the favored coverage is the one for which the number of μ coordinated H and CO is the highest. Multicarbonyl sites arise when the global coverage exceeds 1 ML.

4 Discussion

We have found that H_2 cannot compete with CO during the adsorption process on the substrate, even when considering adsorption energies only, *i.e.* without taking into consideration activated grafting. Owing to the large differences in adsorption energies between the two adsorbates, under a 1 bar pressure of H_2, H-only covered RuNPs are expected for low pressures of CO (for instance, below *ca.* 10^{-7} bar at $T = 450$ K). Regarding kinetics, which were not considered in the present study, one can refer for example to a recent experimental work, dealing with the initial dissociation probability of D_2 on Ru(0001) as a function of its kinetic energy for various CO pre-coverages between 0.00 and 0.67 ML at a temperature of 180 K, studied by molecular-beam techniques.[72] The results indicated that CO blocks D_2 dissociation and that non-activated sticking and dissociation become less important with increasing CO coverage, and vanishes at 0.33 ML. However, at D_2 kinetic energy higher than 8 kcal.mol^{-1} the site-blocking capability of CO decreases rapidly. Coming back to the colloidal context, there is a puzzling contradiction with the lack of hydrides suggested by our calculations and the capability of small RuNPs to be efficient FTS catalysts, a reaction which obvi-

ously requires H atoms and CO groups. It could *a priori* be related to the chosen methodologies, *i.e.* either the DFT functional, the lack of kinetically-based sticking energies, or the simplicity of the thermodynamic model. An overestimation of the CO adsorption energy due the DFT functional does not seem to account for this apparent discrepancy. New phase diagrams have indeed been calculated after tuning the adsorption energies per CO or H ligand, as reported in Figure S9. A lowering by *ca.* 13% of CO adsorption energies (*i.e.* ~ 7 kcal.mol^{-1} per CO), does not enlarge the coexistence domain of the two adsorbates. It is shifted to higher p_{CO} values, but under a 3 bar pressure of syngas, carbon monoxide is still expected to be the only grafted species on the surface, with 1.3 CO/Ru$_{surf}$. By performing partially relaxed potential energy surface scans, we have also tried to estimate a possible cooperative/uncooperative effect during the adsorption of CO on an hydrogenated surface or conversely during the adsorption of H$_2$ on a carbonylated surface. No such effect seems to facilitate the adsorption of H$_2$ or to hamper the adsorption of CO. The resulting energy curves, reported in the SI (Figure S10), show a barrierless adsorption of CO on an hydrogen-saturated RuNP, whereas CO and H$_2$ adsorb on Ru$_{55}$(CO)$_{65}$ with a low barrier height (~ 10 kcal.mol^{-1} and 12 kcal.mol^{-1} respectively).
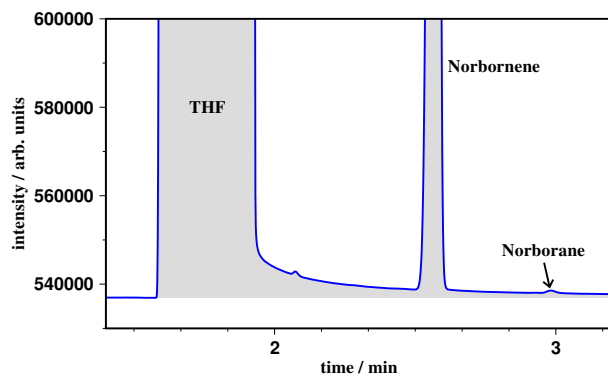
Fig. 10 Gas chromatography spectrum recorded after reaction of 37.5 mg of 2-norbornene with 100 mg of RuNP@PVP in a 80 mL Fischer-Porter tube obtained under 3 bar of syngas at 150 °C

This result led us to start doing new titration experiments. [33,47,63] As recalled earlier, the titration of surface hydrides can indeed be achieved via the estimation of olefin conversion into alkanes. [31] 1.3 nm RuNPs@PVP previously exposed to syngas at 3 bar (1:1 molar mixture of H$_2$ and CO) and 80°C or 150°C have not been able to convert norbornene into norborane, thus proving experimentally an insignificant amount of H atoms coordinated on the surface, which are found as traces (Figure 10). This experimental result confirms that the FTS reaction occurs on CO-saturated RuNPs which accommodate a very low amount of H atoms, if any. It is not in contradiction with a recent work dealing with silica-supported RuNPs, which was not able to decide

if the presence of surface hydrides could result from remaining chemisorbed hydrogen even upon pretreatment of the sample at 350 °C and 10^{-5} mbar prior adsorption of ^{13}CO, or alternatively could being formed by reaction of surface silanol groups with surface Ru atoms in contact with the silica surface. [55] According to our joint experimental/theoretical study, the latter assumption is more likely. This is a very important result regarding the initiation of the CO consumption reaction. Yet, the H-assisted route has been shown to facilitate CO dissociation, whereas barriers for the unassisted dissociation channel are significantly higher. It has also been reported that direct CO dissociation is inconsistent with reported FTS rate equations. [14] Moreover, at high CO coverage CO desorption/adsorption is fast, as shown in the same article by a microkinetics model. Another recent work based on microkinetics simulations predicted that surface coverages are dominated by CO, C and O, according to the reactivity regime (CO dissociation, chain growth termination, or water removal, respectively). [73] Overall, these results suggest that the dissociative adsorption of H$_2$ on CO-saturated RuNP surfaces is a rare event, and that the progressive formation of transient species, resulting for example from a substantial O coverage [73] among other assumptions, could then facilitate the adsorption of H$_2$ after an uneasy initiation of the reaction. At the atomic scale, the first steps of the Fischer-Tropsch reaction should be modeled on a RuNP with a high coverage of CO and a very low number of hydrides. Such study is under progress in our group.
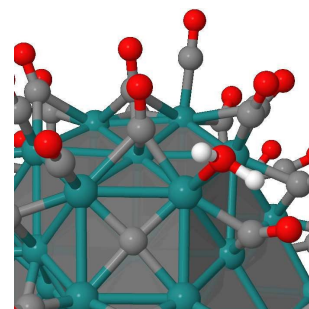
Fig. 11 (a) Possible carbide-water reaction intermediate (Ru$_{55}$(CO)$_{65}$(C)(H$_2$O)) of the Fischer-Tropsch reaction

However, we shall now consider one reaction intermediate, that could possibly be encountered on the H-assisted or carbide pathways, and which design results from the analysis of the ε_d and IpCOHP energy indexes and from the lack of hydrides on the surface in a significant amount. The underlying idea is to consider that a thermodynamic driving force may favor the coordination of a dihydrogen molecule on a CO-saturated ruthenium surface. The intermediate reported in Figure 11 results from the reaction Ru$_{55}$(CO)$_{66}$ + H$_2$ $\longrightarrow$ Ru$_{55}$(CO)$_{65}$(C)(H$_2$O) (reaction 1), that would occur at the interface between the (001) and (101) planes. It exhibits a μ_5-carbide which lies in the ruthenium sur-

face and which is both coordinated to four surface Ru atoms and to a core Ru atom. This insertion is facilitated by a lowering of the Ru-Ru bond strength and by the *d*-band center of the core atom which high value may not work again the partial insertion of an atom. Due to the saturation of the surface by CO ligands, Ru-Ru bond lengths of the four-fold site are significantly elongated with respect to the bare RuNP, and it is even more pronounced after the C-insertion ($Ru_{55}(CO)_{65}(C)(H_2O)$: ~2.81 Å; $Ru_{55}(CO)_{66}$: ~2.75 Å; Ru_{55}: ~2.64 Å). This reaction is exothermic by 22 kcal.mol^{-1}, partly due to the adsorption energy of H_2O (~17 kcal.mol^{-1}). According to this rather large exothermicity, this reaction is competitive with the adsorption/desorption of CO equilibrium (the adsorption of one additional CO to $Ru_{55}(CO)_{66}$ is exothermic by ~20 kcal.mol^{-1} only, instead of ~50 kcal.mol^{-1} on the bare Ru_{55} cluster). The resulting phase diagram, plotted in Figure 12, confirms that the formation of such stable intermediate competes with the sole adsorption of carbon monoxide.
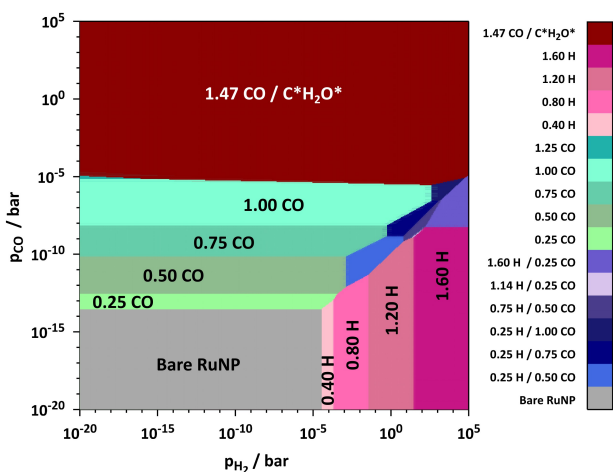
Fig. 12 Phase diagram for H_2 and CO adsorption on a 1nm RuNP at 450 K. The diagram differs from Figure 6 by taking into account $Ru_{55}(CO)_{65}(C)(H_2O)$ (red domain)

It is also interesting to notice that the hypothetical reaction $Ru_{55}(CO)_{66} + H_2 \longrightarrow Ru_{55}(CO)_{65}(C) + H_2O$, (reaction 2), is exothermic by 5 kcal.mol^{-1}, in line with the high *d*-band center value of the Ru core atoms. From a thermodynamic point of view, and provided that kinetics do not impede it, the dissociation of C-O immediately followed by the formation of water on the surface could favor the adsorption of H_2. The picture on the bare Ru_{55} cluster is very different. The counterpart of reaction 1, $Ru_{55}(CO) + H_2 \longrightarrow Ru_{55}(C)(H_2O)$, is almost athermic (-1 kcal.mol^{-1}), whereas reaction 2 becomes endothermic by 11 kcal.mol^{-1}. Since the adsorption energy of water is similar to the $Ru_{55}(CO)_{66}$ case (-12 kcal.mol^{-1}), this 11 kcal.mol^{-1} value can be attributed to an unfavorable coordination of the carbide in a fourfold site of the surface. Besides, the carbide lies above the sur-

face and it is not anymore coordinated to a ruthenium core atom, both in $Ru_{55}(C)(H_2O)$ and in $Ru_{55}(C)$. This analysis further confirms that surface species possibly involved in the Fischer-Tropsch mechanism may not have the same geometries nor the same adsorption energies on a surface saturated with CO and on a bare surface, due to electronic effects.

5 Conclusion

The present work is a computational chemistry study of the surface composition of ruthenium NPs blended with a systematic analysis of their wavefunction, thanks to electronic descriptors (pDOS, *d*-band center, COHP, IpCOHP). Considering the simultaneous adsorption of H_2 and CO on nanocatalysts is an important scientific goal, owing to its relevance to the Fischer-Tropsch synthesis and the methanation reaction. The H_2:CO surface composition of Ru_{55}, a 1 nm RuNP, exposed to syngas has been evaluated according to a thermodynamic model fed with DFT energies and vibrational frequencies that account for ZPE contributions to energies. This *ab initio* thermodynamics method provides a connection between the microscopic and macroscopic regimes since it gives the preferred surface composition as a function of environmental conditions, provided that no relevant structural assumption has been neglected in the sampled structures. This study aims at designing a model of RuNPs covered with a relevant CO:H_2 stoichiometry. As already underlined by us in a recent mechanistic study dealing with an enantiospecific C-H activation using ruthenium nanocatalysts,[74] computational chemistry calculations need to be performed on relevant structural models, *i.e.* with a realistic surface - and possibly subsurface - composition. Yet, in the context of ultra small and small NPs, slab models cannot account for actual NPs, owing to different electronic features and to the presence of edges and apexes on the surface, which may involve different surface compositions.

The experimental access to these informations requires the use of several techniques of characterization, sometimes in conjunction with DFT or theoretical models in order to secure the assignation of experimental data (high energy XRD, NMR, XPS, IR, GC...). The surface compositions provided by the *ab initio* thermodynamics method used in the present work are accurate enough to state that it can support experiments and should be used as part of a multiscale strategy aiming at evaluating the catalytic, optic or magnetic properties of organometallics NPs. The phase diagrams given in this study are relevant both in the organometallic synthesis context (*p* near 1 bar and *T* near room temperature or higher) and in the sputtering production context (*p* near 10^{-7} bar and low *T*). The resulting phase diagrams have been systematically compared with experimental data,[31,33,47,63] as well as with a very recent combined experimental/theoretical work dealing with the surface composition of RuNPs under H_2 or CO atmospheres, but which did not consider a possible co-

adsorption at the DFT level.[55] In order to evaluate the ratio of surface hydrides at temperatures relevant to FTS conditions on RuNPs, new titration experiments have been done at 80°C and 150°C in addition to the experimental compositions previously published.[33,63] According to *ab initio* thermodynamics, RuNPs accommodate 1.5 H per surface Ru atom under an H_2 pressure of 3 bar at r.t., a somewhat higher coverage value than usually admitted on the Ru(0001) surface.[26] When hypothetically submitted to a pressure of CO of 2 bar at r.t., naked RuNPs are covered with 1.5 CO per surface Ru atom. When exposed to a mixture of H_2 and CO, phase diagrams show only a very small domain of coexistence of both adsorbates on the surface at very low pressures of carbon monoxide. At 450 K and 3 bar of syngas, a high amount of CO (1-1.5 ML) is expected to be found on the surface, but without any H. This is in full agreement with new experiments, which have showed that only traces of hydrides can be found on the surface of small RuNPs, even at 150°C, *i.e.* a temperature slightly below the Fischer-Tropsch synthesis on these nanocatalysts. These findings shed a new light on the possible reaction pathways underlying the FTS, and specifically the initiation of the reaction.

Thanks to an analytic projection from plane augmented wave (PAW) wavefunctions onto a localized Slater basis set, an added value of the present work is the analysis of the DOS and of the COHP, an atom-resolved chemical bonding indicator. Together with the *d*-band center model, the COHP index has been successfully compared to IR data and systematically used to interpret adsorption energies. We also show that these energy descriptors can be used in order to design reaction intermediates that could be involved in the complex mechanism that underlies the Fischer-Tropsch reaction. We suggest that the simultaneous dissociation of CO and formation of water could be a thermodynamic driving force regarding H_2 coordination. The interesting outcome of this reaction would be a μ_5 carbide, which relative stability depends on the surface coverage.

The Fischer-Tropsch reaction network is complex, its mechanism is still unresolved, and the present study opens new questions. Since ultrasmall RuNPs have a low activity with respect to FTS,[31] it would be interesting in a further theoretical study to evaluate the role of other surface ligands, such as dppb, on the catalytic activity of larger RuNPs: do they modulate the electronic structure of the metal catalysts? Do they favor the presence of special sites? Is there a cooperative effect between them and hydrides that would increase the H:CO ratio?.

Possible kinetic effects during the adsorption process may arise in experiments, whereas the *ab initio* thermodynamics method is based on an equilibrium assumption. Even if in the present study these phase diagrams account with the experimental findings, kinetically-activated adsorption processes could be more important with other ligands or metals. Consideration of such effects will be the scope of our next study.

6 Theoretical and experimental methods and models

6.1 Modeling the nanoparticles

RuNPs exist in a wide range of shapes and sizes, from small spherical ($\sim$1.0 nm) hcp nanoparticles to larger rod-like structures, according to the synthesis conditions and more particularly due to the stabilizer used for their preparation. For instance, ultrasmall 1 nm RuNPs were produced using a betaine adduct of N-heterocyclic carbene and carbodiimide as stabilizer,[34] whilst 1.3 nm and 2.3 nm spherical RuNPs were obtained using respectively the PVP polymer[51] or an octylamine ($C_8H_{17}NH_2$).[75] It is also noteworthy that, when alkylamine ligands are used as stabilizers, the decomposition of the ruthenium precursor in mild conditions leads to nanoparticles of different shapes according to the length of the carbon chain. Thus, classical spherical RuNPs are obtained using $C_8H_{17}NH_2$ as stabilizer whereas a rod-like structures are obtained using $C_{12}H_{25}NH_2$ or $C_{16}H_{33}NH_2$. Although RuNPs exhibit hcp structures, to the best of our knowledge there is a unique exception of synthesized fcc RuNPs, between 2.4 and 5.4 nm.[76]

Most of the time, slab models are used to describe large nanoparticles, since their facets can suitably be described by an infinite surface,[14,77] but in the case of small nanoparticles ($\lesssim 3$ nm), the slab model becomes fairly relevant, as the surface of the nanoparticle does not exhibit large, regular facets and as a so-called quantum-size effect is expected to occur.[78] We chose to focus on a 1 nm 55-atoms hcp cluster, which is slightly smaller than the experimental RuNP@PVP we shall often refer to in the present article. The shape is mainly spherical but its surface is shaped to mimic irregularities that probably statistically exist in a collection of small hcp nanoparticles. This average representation of small RuNPs differs from the perfect hcp crystal considered by Comas-Vives *et al.*[55], which exhibits two (001) planes and twelve (101) planes. As shown in Figure 1, our model is also a spherical hcp crystal shaped by slicing an hcp structure by two (001) planes and (101) planes. A tip has been added in order to introduce a B4 and a B5 sites. Removing one line of atoms between two (101) planes generates a slightly corrugated facet. In that way, we aim at designing a versatile model of Ru catalysts that could experimentally be involved in Fischer-Tropsch synthesis.

We have considered several adsorptions sites: top sites (η) where the ad-ligand is adsorbed above one surface Ru atom, bridging sites (μ) where the ad-ligand is coordinated to two surface Ru atoms, three-fold face capping sites (μ_3) where the ad-ligand is adsorbed on a triangular facet, four-coordinated sites (μ_4) where the ad-ligand is simultaneously adsorbed on four metal atoms. In the case of CO a coordination mode for which both C and O adsorbs at the nanoparticle surface (η, η^2) was also considered.

In order to define the bridging character μ_n and the hapticity

η^m, we have considered an atom of the ad-ligand as coordinated to a given metal atom when the metal-atom distance is lower than 2.1 Å for H, 2.5 Å for C and 2.3 Å for O.

6.2 DFT Calculations

All the calculations were performed using the Vienna *ab initio* simulation package, VASP[79,80] within the framework of density functional theory. Projector augmented waves (PAW)[81,82] were used, with a plane-wave kinetic energy cutoff of 500 eV. All the calculations used the Perdew-Burke-Ernzerhof form of the generalized gradient approximation.[57] The supercell used was $27 \times 27.5 \times 28$ Å large, ensuring at least 16 Å of vacuum between to successive images of ligand-covered Ru_{55}. Γ-centered[83] calculations were performed with a Gaussian smearing (σ) of 0.02 eV, the energies being therefore extrapolated for $\sigma = 0.00$ eV. The atoms positions were optimized until the criterion of the residual forces on any direction being less than 0.02 eV/Å was met. Vibrational modes were calculated using the dynamical matrix scripts from Henkelman's group.

The obtained total energies were then used to determine adsorption energies. CO and H_2 do not adsorb in the same way at the nanoparticle surface. Whereas CO adsorbs in its molecular form, H_2 is known to undergo dissociation during the adsorption process. Therefore, the adsorption energies given in this paper are calculated using equation 2, which includes the cost of the H-H bonds breaking. The general formula for a co-adsorption process is:

$$E_{ads}(nL^1, mL^2) = \frac{1}{n+m}[E(M_{55}L_n^1 L_m^2) - E(M_{55}) - \frac{n}{k_1}E(L^1) - \frac{m}{k_2}E(L^2)] \quad (2)$$

where M = Ru ; L^1, L^2 = H_2 ($k = 2$), CO ($k = 1$).

6.3 *ab initio* thermodynamics

It is possible to calculate the free energy and other thermodynamic functions of solids and liquids, using first principles methods. Such method has successfully been applied to explain or predict thermodynamic material properties, and in particular surface properties at the solid-gas interface.[26,35–38]. We have applied this calculation in order to determine a phase diagram depending on the H or CO coverage of the surface on the nanoparticle (from 0.02 to 2.5 ML for H and from 0.02 to 1.70 ML for CO). In practice, the energies of the nanoparticle covered by H or CO, under a wide range of pressure and temperature, is obtained from the $T = 0$ K and $p = 0$ Pa *ab initio* energies of the same nanoparticle. The Gibbs free energy of adsorption per unit area of different ligands on the bare metal nanoparticle (MNP), $\Delta_a G_{NP}(T,p)$, requires to calculate the Gibbs free energy for the reaction $MNP + \sum_i n_i L_i = \sum_i n_i L_i^*$, with the bare nanoparticle chosen as the reference:
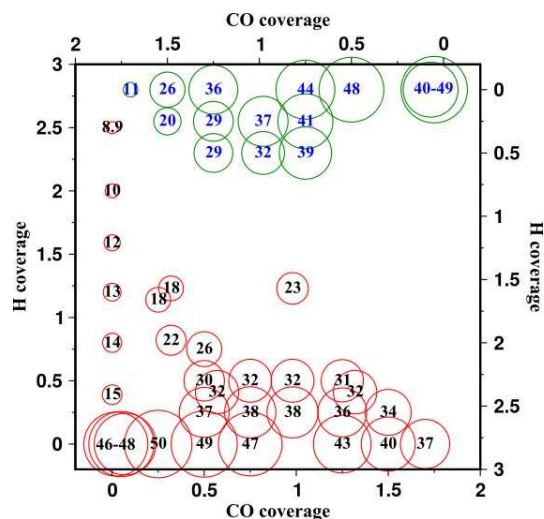
Fig. 13 Lower part (in red and black): average adsorption energies $E_{ads}(nH, mCO)$ (eq. 2, absolute values, in kcal.mol^{-1}). ; upper part (in green and blue): average adsorption energy with respect to another CO coverage (eq. 9, absolute values, in kcal.mol^{-1}). Circles size is proportional to $|E_{ads}|$.

$$\Delta_a G_{NP}(T,p) = \frac{\mu(\sum_i n_i L_i^*, T, p) - \mu(MNP, T, p) - \sum_i n_i \mu_i(T, p)}{A_{NP}} \quad (3)$$

$\Delta_a G$ is normalized per unit area by dividing through the nanoparticle surface area A_{NP}. The use of chemical potentials accounts for the temperature and pressure effect on ligands (L_i) adsorption on the nanoparticle surface for a given metal NP. It is assumed that for condensed phases the difference $\mu(\sum_i n_i L_i^*) - \mu(MNP)$ can be approximated by the difference between the calculated electronic energy including (eq. 4) or not (eq. 5) thermal variations of internal energies, as well as pV terms and entropy contributions. Such approximation has given good results, probably owing to some cancellation of the pressure- and temperature-dependent terms of the condensed phases. Eq. 3 becomes :

$$\Delta_a G = \left[\Delta G^\circ - \sum_i n_i \mu_i(T, p)\right] / (A_{NP}) \quad (4)$$

$$\Delta_a G = \left[\Delta E - \sum_i n_i \mu_i(T, p)\right] / (A_{NP}) \quad (5)$$

The chemical potential for ligands L_i, coming from an external reservoir in equilibrium with the colloidal solution, can then be calculated from the standard chemical potential and the activity of the ligand. In the case of ligands coming from the gas phase such as CO and H_2 in this case, the p-dependence is introduced

in each L_i chemical potential through an ideal gas law. It comes:

$$\mu_i(T,p) = \mu_i^{\ominus}(T,p^{\circ}) + kT \ln(\frac{p_i}{p^{\circ}}) \quad (6)$$

$\mu^{\ominus}(L_i,T,p^{\circ})$ can usually be calculated from H_T° and S_T° values given in thermodynamic tables[84] ($\mu_i^{\ominus}(T,p^{\circ}) = H_i^{\circ}(T) - TS_i^{\circ}(T)$) or computed from first-principles calculations done at 0K. In this case the standard chemical potential, *i.e.* $G_T^{\circ}(L)$, is given by:[85]

$$\mu_i^{\ominus}(T,p^{\circ}) = E^{\text{DFT}}(L_i) + H_{i,\text{therm}}^{\circ}(T) - TS_i^{\circ}(T) \quad (7)$$

By taking into account vibrational contributions, eq. 3 becomes:

$$\Delta_a G = \frac{\Delta E - \sum_i (n_i \mu_i(T,p) + F_{n_i L_i^*}^{\text{vib}})}{A_{\text{NP}}} \quad (8)$$

with $F_{n_i L_i^*}^{\text{vib}} = E_{n_i L_i^*}^{\text{vib}} - TS_{n_i L_i^*}^{\text{vib}}$

Table 1 Calculated vibrational frequencies (cm^{-1}) for several coordination modes on the RuNP.
† subsurface H in an octahedral site.

Coordination type		Frequencies				
	η	1860	400			
	μ	1400	940	630		
Ru-H	μ_3	1300	900	550	500	
	H_2	2230				
	μ_6†	1141	964	785		
	η	1900	506	432	429	
	μ	1750	410	335	305	
Ru-CO	μ_3	1670	350	280	229	
	(η,η^2)	1415	450	380	280	245
	μ_4	1306	460	214		

All these equations have been implemented in a program, *aithermo*, aiming at considering co-adsorption processes. It provides (T,p) phase diagrams which show the most stable surface composition according to $\Delta_a G$ (eq. 8). $\Delta_a G$ can as well be plotted as a function of T or p in order to simultaneously see the evolution of $\Delta_a G$ as a function of the temperature or the pressure. All the diagrams given hereafter are for temperature ranging from 1 K to 1000 K, far below the melting point of ruthenium bulk (2602 K), and pressure from 10^{-20} bar up to 10^5 bar. It accounts for the stability of the adsorbed species without considering kinetics effects. It is also to be noted that the *ab initio* thermodynamics equations use ideal gas law, so the high-pressure part of the diagrams must be considered with caution. For co-adsorption, the *aithermo* code provides phase diagrams either at a given temperature for both ligands pressures varying, or, one ligand pressure can be fixed, depicting the stability domains for the other ligand pressure and the temperature variable.

The H-RuNP vibrational modes taken into account here were obtained by computing the vibrational frequencies on Ru$_{13}$ icosahedral clusters covered with H. The H-H stretching mode for non dissociated adsorbed H$_2$ was also computed in the same way. In the case of CO, we used the mean frequency given by the computation of normal modes on optimized Ru$_{55}$-CO clusters for each type of coordination. The vibrational frequencies used in the *ab initio* thermodynamics equations are listed in Table 1.

All the considered surface compositions, from 0.02 ML (Ru$_{55}$H) to 2.5 ML (Ru$_{55}$H$_{110}$) for the adsorption of H$_2$ and from 0.02 ML (Ru$_{55}$CO) to 1.70 ML (Ru$_{55}$(CO)$_{70}$) for CO are shown in Figures S4 and S7. For a same coverage, different configurations were probed, their description is given in Tables S5 and S6. All considered surface composition are also reported in Figure 13, together with the average adsorption energies with respect to the bare Ru$_{55}$ NP (eq. 2). Another interesting information is provided by the adsorption energy relative to the closest less saturated cluster considered in this study. In that way, the thermodynamic yield corresponding to the adsorption of additional CO ligands on an already hydrogenated and carbonylated surface is also reported in the upper part of Figure 13. It is simply given by, for the addition of p CO ligands to a Ru$_{55}$H$_n$(CO)$_m$:

$$E_{\text{ads}}(n\text{H},m\text{CO}+p\text{CO}) = \frac{1}{p}[E(\text{M}_{55}\text{H}_n(\text{CO})_{m+p}) - E(\text{M}_{55}\text{H}_n(\text{CO})_m) - pE(\text{CO})] \quad (9)$$

In the case of the hydrogen adsorption, coverage values under 1.0 ML exhibit only μ or μ_3 configurations. This differs from results obtained on the flat Ru(0001) surface for which only μ_3 coordination are favored,[26] but it agrees with results on an hcp cluster where μ adsorption was found to be the most stable even at higher coverages.[55] Atop hydrides appear above 1 ML, in agreement with previous results obtained on Ru(0001) where the most stable configurations were found for total occupation of the fcc sites followed by top sites. For high CO coverages, the preferred coordination modes are η and μ. This is still true for coverages under 1.00 ML where structures with mixed η and μ coordinated CO are more stable than with only η adsorptions.

6.4 Analysis of the electronic structure

One of the cornerstones of quantum chemistry is its ability to provide simple and powerful models able to rationalize phenom-

ena. It has been shown in several studies that the adsorption strength of chemical species on metal surfaces can be understood in terms of Hammer and Nørskov's d-band center model: the closer to the Fermi level the d-band center of a metal surface, the higher the adsorption energy of ligands. [6,43–45] But this model is only related on energies and it lacks explicit information on the electronic structure. Yet, although VASP is well suited for efficiently calculating the wavefunction of metal systems, it works in reciprocal space, which makes the quantum chemical information not easy to handle. This is why Hoffmann proposed the crystal orbital overlap population (COOP) concept, [48,69] based on Extended Hückel theory, and which provides an overview of the bond strength in crystals and of the bonding $vs.$ antibonding character of the states. The crystal orbital hamilton population (COHP) was then introduced in the framework of DFT by Dronskowski and Blöchl. [46] COHP is a partitioning of the band-structure energy in terms of orbital-pair contributions, and it is therefore based on a local basis (eq. 10).

$$\mathrm{COHP}_{\mu\nu}(\varepsilon) = \sum_{n\mathbf{k}} c_{\mu}^{*} c_{\nu} H_{\mu\nu} \delta\left(\varepsilon - \varepsilon_n(\mathbf{k})\right) \qquad (10)$$

The Lobster package which has been used in this work, [86,87] allows to calculate COHP curves projected in a local atomic basis set (pCOHP), and also reliable atom-projected density of states (pDOS), both directly based on plane-wave DFT output as given by the VASP package.

The d-band center, ε_d, is computed as the normalized, energy-weighted integral of the density of states (DOS), projected onto all d atomic orbitals (AOs) of a selected set of metal atoms:

$$\varepsilon_d = \frac{\sum_\alpha \sum_m \int_{E_{\min}}^{E_\mathrm{F}} \varepsilon\, n_{d_m}(\alpha, \varepsilon)\, d\varepsilon}{\sum_\alpha \sum_m \int_{E_{\min}}^{E_\mathrm{F}} n_{d_m}(\alpha, \varepsilon)\, d\varepsilon} \qquad (11)$$

where m runs over the five d AOs and $n_{d_m}(\alpha, \varepsilon)$ is the atom-projected density of states on the d_m AO of atom α. We chose to integrate up to the Fermi energy, as previously proposed by us, [45] which is a lower bound for the d-band center usually calculated. In that previous study the DOS was projected with VASP. Yet it uses identical Wigner-Seitz spheres for all orbitals of a given atomic species, which does not comply with the different spatial extent of these atomic orbitals. We now use the pDOS calculated with the Lobster program. A comparison done on some test cases does not show large differences between the ε_d values calculated with both approaches. The pCOHP and pDOS properties obtained for the $\mathrm{Ru_4H_4(CO)_{12}}$ and $\mathrm{Ru_4H_4(C_6H_6)_4}$ clusters with different basis sets were carefully analyzed and compared to their well-known molecular orbitals. [50] The so-called pbeVASPfit basis set of Lobster was chosen for Ru, with additional $5p$ functions({$4p$, $4d$, $5s$, $5p$}). Otherwise mentioned, and owing to the lack of symmetry and to the absence of a privileged adsorption facet on the contrary to slab models, COHP profiles between two types of atoms

were calculated by taking into account all their valence AOs.

For hydrogenated and/or carbonylated species, the basis set was completed with $1s$ function on each H atom and $2s$ and $2p$ functions on each C and O atoms. Owing the atomic basis set on which the projection is achieved, the calculation of at least $12n + m + 8k$ bands is necessary for a $\mathrm{Ru_{55}H_m(CO)_k}$ compound. Note that for all compounds considered in this work, the charge spilling, a criterion that assesses the quality of the projection, is systematically lower than 0.7%. The integrated pCOHP (IpCOHP $= \int_{E_{\min}}^{E_\mathrm{F}} \mathrm{pCOHP}(\varepsilon)d\varepsilon$), calculated in some cases, provides a qualitative information of the average bond strength in covalent systems.

6.5 Experimental hydride titration

Following the experimental procedure proposed by Martínez-Prieto $et\ al.$ [31], a Fischer-Porter (80 mL) vessel was filled with 100 mg of 1.3nm $\pm$ 0.2nm RuNPs@PVP ($\sim$8% Ru), pressurized with 3 bar of syngas (1:1 molar mixture of H_2 and CO) and heated either at 80°C and 150°C for 24 h. The hydrides adsorbed were then quantified following a previously reported procedure, which consists in the titration of surface hydrides with norbornene and measure the amount of alkane formed. [63] The Fischer-Porter vessel is depressurized at 80°C or 150°C. After that, the RuNPs@PVP are re-dispersed in 10 mL of THF and react with 2-norbornene (37.5 mg, 0.4 mmol, 5 equiv.). After 24h of vigorous stirring in a 10 ml flask, the amount of norbornane formed is measured by gas chromatography (GC) analysis.

References

1　F. Fischer, $Brennst.\ Chem.$, 1921, **2**, 386–387.

2　H. Schulz, $Appl.\ Catal.,\ A$, 1999, **186**, 3–12.

3　E. van Steen and M. Claeys, $Chem.\ Eng.\ Technol.$, 2008, **31**, 655–666.

4　X.-Y. Quek, Y. Guan, R. A. van Santen and E. J. M. Hensen, $ChemCatChem$, 2011, **3**, 1735–1738.

5　I. A. W. Filot, R. A. van Santen and E. J. M. Hensen, $Catal.\ Sci.\ Technol.$, 2014, **4**, 3129–3140.

6　B. Hammer, Y. Morikawa and J. K. Nørskov, $Phys.\ Rev.\ Lett.$, 1996, **76**, 2141–2144.

7　O. R. Inderwildi, S. J. Jenkins and D. A. King, $J.\ Phys.\ Chem.\ C$, 2008, **112**, 1305–1307.

8　F. Fischer and H. Tropsch, $Brennst.\ Chem.$, 1923, **4**, 276–285.

9 F. Fischer and H. Tropsch, *Brennst. Chem.*, 1926, **7**, 97–104.

10 S. R. Craxford, *Trans. Faraday Soc.*, 1946, **42**, 576–580.

11 P. Biloen, J. N. Hell and W. M. H. Sachtler, *J. Catal.*, 1979, **42**, 95–107.

12 P. Biloen and W. M. H. Sachtler, *Adv. Catal.*, 1981, **30**, 165–216.

13 S. Shetty, A. P. J. Jansen and R. A. van Santen, *J. Phys. Chem. C*, 2009, **113**, 19749–19752.

14 B. T. Loveless, C. Buda, M. Neurock and E. Iglesia, *J. Am. Chem. Soc.*, 2013, **135**, 6107–6121.

15 J. L. C. Fajin, M. N. D. S. Cordeiro and J. R. B. Gomes, *Catalysts*, 2015, **5**, 3.

16 S. Shetty and R. A. van Santen, *Catal. Today*, 2011, **171**, 168–173.

17 M. Andersson, F. Abild-Pedersen, I. Remediakis, T. Bligaard, G. Jones, J. Engbk, O. Lytken, S. Horch, J. Nielsen, J. Sehested, J. Rostrup-Nielsen, J. Nørskov and I. Chorkendorff, *J. Catal.*, 2008, **255**, 6–19.

18 M. Ojeda, R. Nabar, A. U. Nilekar, A. Ishikawa, M. Mavrikakis and E. Iglesia, *J. Catal.*, 2010, **272**, 287–297.

19 H. Li, G. Fu and X. Xu, *Phys. Chem. Chem. Phys.*, 2012, **14**, 16686–16694.

20 H. Pichler and H. Schulz, *Chem. Ing. Tech.*, 1970, **42**, 1162–1174.

21 G. Henrici-Olivé and S. Olivé, *Angew. Chem. Int. Ed.*, 1976, **15**, 136–141.

22 H. H. Storch, N. Golumbic and R. B. Anderson, *The Fischer-Tropsch and Related Syntheses*, John Wiley & Sons, Inc., New York, 1951.

23 I. M. Ciobîcă, A. W. Kleyn and R. A. van Santen, *J. Phys. Chem. B*, 2003, **107**, 164–172.

24 X.-Y. Quek, I. A. W. Filot, R. Pestman, R. A. van Santen, V. Petkov and E. J. M. Hensen, *Chem. Comm.*, 2014, **50**, 6005–6008.

25 M. Y. Chou and J. R. Chelikowsky, *Phys. Rev. Lett.*, 1987, **59**, 1737–1740.

26 I. del Rosal, L. Truflandier, R. Poteau and I. C. Gerber, *J. Phys. Chem. C*, 2011, **115**, 2169–2178.

27 B. Riedmüller, I. M. Ciobîcă, D. C. Papageorgopoulos, F. Frechard, B. Berenbak, A. W. Kleyn and R. A. van Santen, *J. Chem. Phys.*, 2001, **115**, 5244–5251.

28 K. Honkala, A. Hellman, I. N. Remediakis, A. Logadottir, A. Carlsson, S. Dahl, C. H. Christensen and J. K. Nørskov, *Science*, 2005, **307**, 555–558.

29 I. M. Ciobîcă and R. A. van Santen, *J. Phys. Chem. B*, 2003, **107**, 3808–3812.

30 S. B. Vendelbo, M. Johansson, D. J. Mowbray, M. P. Andersson, F. Abild-Pedersen, J. H. Nielsen, J. K. Nørskov and I. Chorkendorff, *Top. Catal.*, 2010, **53**, 357–364.

31 L. M. Martínez-Prieto, S. Carenco, C. H. Wu, E. Bonnefille, S. Axnanda, Z. Liu, P. F. Fazzini, K. Philippot, M. Salmeron and B. Chaudret, *ACS Catal*, 2014, **4**, 3160–3168.

32 J. M. G. Carballo, J. Yang, A. Holmen, S. Garcia-Rodriguez, S. Rojas, M. Ojeda and J. L. G. Fierro, *J. Catal.*, 2011, **284**, 102–108.

33 F. Novio, K. Philippot and B. Chaudret, *Catal. Lett*, 2010, **140**, 1–7.

34 L. M. Martínez-Prieto, C. Urbaneja, P. Palma, J. Cámpora, K. Philippot and B. Chaudret, *Chem. Comm.*, 2015, **51**, 4647–4650.

35 K. Reuter and M. Scheffler, *Phys. Rev. B*, 2001, **65**, 035406.

36 W.-X. Li, C. Stampfl and M. Scheffler, *Phys. Rev. B*, 2003, **68**, 165412.

37 C. Arrouvel, M. Digne, M. Breysse, H. Toulhoat and P. Raybaud, *J. Catal.*, 2004, **222**, 152–166.

38 K. Reuter, C. Stampfl and M. Scheffler, in *Handbook of Materials Modeling*, ed. S. Yip, Springer, Berlin, Heidelberg, 2005, vol. 1, ch. *ab initio* atomistic thermodynamics and statistical mechanics of surface properties and functions, pp. 149–194.

39 D. Schooss, M. N. Blom, J. H. Parks, B. v. Issendorff, H. Haberland and M. M. Kappes, *Nano Lett.*, 2005, **5**, 1972–1977.

40 E. Waldt, R. Ahlrichs, M. M. Kappes and D. Schooss, *ChemPhysChem*, 2014, **15**, 862–865.

41 S. M. Lang, T. M. Bernhardt, M. Krstić and V. Bonačić-Koutecký, *Angew. Chem., Int. ed. Eng.*, 2014, **53**, 5467–5471.

42 E. Waldt, A.-S. Hehn, R. Ahlrichs, M. M. Kappes and D. Schooss, *J. Chem. Phys.*, 2015, **142**, 024319.

43 B. Hammer and J. K. Nørskov, *Surf. Sci.*, 1995, **343**, 211–220.

44 B. Hammer and J. Nørskov, in *Impact of Surface Science on Catalysis*, ed. B. C. Gates and H. Knozinger, Academic Press, 2000, vol. 45, pp. 71–129.

45 I. del Rosal, M. Mercy, I. C. Gerber and R. Poteau, *ACS Nano*, 2013, **7**, 9823–9835.

46 R. Dronskowski and P. E. Blöchl, *J. Phys. Chem.*, 1993, **97**, 8617–8624.

47 F. Novio, D. Monahan, Y. Coppel, G. Antorrena, P. Lecante, K. Philippot and B. Chaudret, *Chem. Eur. J.*, 2014, **20**, 1287–1297.

48 T. Hughbanks and R. Hoffmann, *J. Am. Chem. Soc.*, 1983, **105**, 3528–3537.

49 W. V. Glassey and R. Hoffmann, *J. Chem. Phys.*, 2000, **113**, 1698–1704.

50 I. del Rosal, F. Jolibois, L. Maron, K. Philippot, B. Chaudret and R. Poteau, *Dalton Trans.*, 2009, 2142–2156.

51 K. Philippot, P. Lignier and B. Chaudret, in *Organometallic Ruthenium Nanoparticles and Catalysis*, ed. P. H. Dixneuf and

C. Bruneau, Springer International Publishing, Switzerland, 2014, vol. 48, pp. 319–370.

52 M. Y. Chou and J. R. Chelikowsky, *Phys. Rev. B*, 1989, **39**, 5623.

53 L. Xu, H. Xiao and X. Zu, *Chem. Phys.*, 2005, **315**, 155–160.

54 I. del Rosal, *Ph.D. thesis*, Université de Toulouse, France, 2009.

55 A. Comas-Vives, K. Furman, D. Gajan, M. C. Akatay, A. Lesge, F. Ribeiro and C. Copéret, *Phys. Chem. Chem. Phys.*, 2016, **18**, 1969–1979.

56 J. Fuggle, T. Madey, M. Steinkilberg and D. Menzel, *Surface Science*, 1975, **52**, 521–541.

57 J. P. Perdew, K. Burke and M. Ernzerhof, *Phys. Rev. Lett.*, 1997, **78**, 1396.

58 M. J. Frisch, G. W. Trucks, H. B. Schlegel, G. E. Scuseria, M. A. Robb, J. R. Cheeseman, G. Scalmani, V. Barone, B. Mennucci, G. A. Petersson, H. Nakatsuji, M. Caricato, X. Li, H. P. Hratchian, A. F. Izmaylov, J. Bloino, G. Zheng, J. L. Sonnenberg, M. Hada, M. Ehara, K. Toyota, R. Fukuda, J. Hasegawa, M. Ishida, T. Nakajima, Y. Honda, O. Kitao, H. Nakai, T. Vreven, J. A. Montgomery, Jr., J. E. Peralta, F. Ogliaro, M. Bearpark, J. J. Heyd, E. Brothers, K. N. Kudin, V. N. Staroverov, R. Kobayashi, J. Normand, K. Raghavachari, A. Rendell, J. C. Burant, S. S. Iyengar, J. Tomasi, M. Cossi, N. Rega, J. M. Millam, M. Klene, J. E. Knox, J. B. Cross, V. Bakken, C. Adamo, J. Jaramillo, R. Gomperts, R. E. Stratmann, O. Yazyev, A. J. Austin, R. Cammi, C. Pomelli, J. W. Ochterski, R. L. Martin, K. Morokuma, V. G. Zakrzewski, G. A. Voth, P. Salvador, J. J. Dannenberg, S. Dapprich, A. D. Daniels, O. Farkas., J. B. Foresman, J. V. Ortiz, J. Cioslowski and D. J. Fox, *Gaussian 09 Revision D.01*, Gaussian Inc. Wallingford CT 2009.

59 W. J. Hehre, R. Ditchfield and J. A. Pople, *J. Chem. Phys.*, 1972, **56**, 2257–2261.

60 M. Scheffler and C. Stampfl, in *Handbook of Surface Science*, ed. K. Horn and M. Scheffler, Elsevier, Amsterdam, 2000, vol. 2, ch. Theory of adsorption on metal substrates, pp. 286–356.

61 G. Blyholder, *J. Phys. Chem.*, 1964, **68**, 2772–2777.

62 T. Pery, K. Pelzer, G. Buntkowsky, K. Philippot, H. H. Limbach and B. Chaudret, *ChemPhysChem*, 2005, **6**, 605–607.

63 J. García-Antón, M. R. Axet, S. Jansat, K. Philippot, B. Chaudret, T. Pery, G. Buntkowsky and H.-H. Limbach, *Angew. Chem., Int. ed. Eng.*, 2008, **47**, 2074–2078.

64 H. Pfnür, P. Feulner, H. Engelhardt and D. Menzel, *Chem. Phys. Lett.*, 1978, **59**, 481–486.

65 H. Pfnür and D. Menzel, *J. Chem. Phys.*, 1983, **79**, 2400–2410.

66 H. Pfnür, D. Menzel, F. M. Hoffmann, A. Ortega and A. M. Bradshaw, *Surf. Sci.*, 1980, **93**, 431–452.

67 A. Stroppa and G. Kresse, *New J. Phys.*, 2008, **10**, 063020.

68 J. A. Herron, S. Tonelli and M. Mavrikakis, *Surf. Sci.*, 2013, **614**, 64–74.

69 R. Hoffmann, *Solids And Surfaces. A Chemist's View of Bonding in Extended Structures*, Wiley-VCH, Weinheim, 1988.

70 V. E. Antonov, I. T. Belash, V. Y. Malyshev and E. G. Ponyatovsky, *Int. J. Hydrogen Energy*, 1986, **11**, 193–197.

71 A. Bradshaw and F. Hoffmann, *Surf. Sci.*, 1978, **72**, 513–535.

72 H. Ueta, I. M. N. Groot, M. A. Gleeson, S. Stolte, G. C. McBane, L. B. F. Juurlink and A. W. Kleyn, *ChemPhysChem*, 2008, **9**, 2372–2378.

73 I. A. W. Filot, R. A. van Santen and E. J. M. Hensen, *Angew. Chem. Int. Ed.*, 2014, **53**, 12746–12750.

74 C. Taglang, L. M. Martínez-Prieto, I. del Rosal, L. Maron, R. Poteau, K. Philippot, B. Chaudret, S. Perato, A. Sam Lone, C. Puente, C. Dugave, B. Rousseau and G. Pieters, *Angew. Chem., Int. ed. Eng.*, 2015, **54**, 10474–10477.

75 C. Pan, K. Pelzer, K. Philippot, B. Chaudret, F. Dassenoy, P. Lecante and M.-J. Casanove, *J. Am. Chem. Soc.*, 2001, **123**, 7584–7593.

76 K. Kusada, H. Kobayashi, T. Yamamoto, S. Matsumura, N. Sumi, K. Sato, K. Nagaoka, Y. Kubota and H. Kitagawa, *J. Am. Chem. Soc.*, 2013, **135**, 5493–5496.

77 B. C. Han, C. R. Miranda and G. Ceder, *Phys. Rev. B*, 2008, **77**, 075410–1–1.

78 *Nanoparticles. From theory to application*, ed. G. Schmid, Wiley-VCH, Weinheim, Germany, 2nd edn., 2010.

79 G. Kresse and J. Fürthmuller, *Phys. Rev. B*, 1996, **54**, 11169–11186.

80 G. Kresse and J. Fürthmuller, *Comput. Mater. Sci.*, 1996, **6**, 15–50.

81 P. Blöchl, *Phys. Rev. B*, 1994, **50**, 17953–17979.

82 G. Kresse and D. Joubert, *Phys. Rev. B*, 1999, **59**, 1758–1775.

83 H. J. Monkhorst and J. D. Pack, *Phys. Rev. B*, 1976, **13**, 5188–5192.

84 D. R. Stull and H. Prophet, *JANAF Thermochemical Tables*, U.S. National Bureau of Standards, 1971.

85 D. A. McQuarrie, *Statistical Mechanics*, University Science Books, Sausalito, California (USA), 2nd edn., 2000.

86 V. L. Deringer, A. L. Tchougréeff and R. Dronskowski, *J. Phys. Chem. A*, 2011, **115**, 5461–5466.

87 S. Maintz, V. L. Deringer, A. L. Tchougréeff and R. Dronskowski, *J. Comp. Chem.*, 2013, **34**, 2557–2567.

Nanoscale Accepted Manuscript